

Massive particle pair production and oscillation in Friedman Universe: reheating energy and entropy, and cold dark matter

She-Sheng Xue

ICRANet Piazzale della Repubblica, 10 -65122, Pescara, Italy
Physics Department, Sapienza University of Rome, Rome, Italy
INFN, Sezione di Perugia, Perugia, Italy
ICTP-AP, University of Chinese Academy of Sciences, Beijing, China
E-mail: xue@icra.it and shesheng.xue@gmail.com

Abstract. Suppose that the early Universe starts with a cosmological Λ -term originating from quantum spacetime at the Planck scale. Dark energy drives inflation and reheating by reducing its value for massive particle-antiparticle pairs production and oscillation, resulting in a holographic and massive pair plasma state. The back-and-forth reaction of dark energy and massive pairs slows inflation to its end and starts reheating by rapidly producing stable and unstable pairs. We introduce the Boltzmann-type rate equation describing the back-and-forth reaction. It forms a close set with Friedman equations and reheating equations for unstable pairs decay to relativistic particles. The numerical solutions show preheating, massive pairs dominated and genuine reheating episodes. We obtain the reheating temperature and entropy in terms of the tensor-to-scalar ratio $0 < r < 0.047$ consistently with observations. Stable massive pairs represent cold dark matter particles and weakly interact with dark energy. The resultant cold dark matter abundance $\Omega_c \sim 10^{-1}$ is about a constant in time.

Contents

1	Introduction	2
2	Slow adiabatic and fast non-adiabatic components	3
3	Quantum massive pair production and oscillation	4
3.1	Quantum massive pair production	4
3.2	Quantum massive pair oscillation	6
4	Massive pair plasma state and holographic hypothesis	9
4.1	Reasons for a macroscopic description	9
4.2	Effective description of a massive pair plasma state	10
5	Back-and-forth process and cosmic rate equation	12
5.1	Stable massive pairs and cosmic rate equation	12
5.2	Unstable massive pair decay and reheating equation	14
6	Initial conditions and basic equations for reheating	15
7	Different episodes in reheating epoch	17
7.1	Preheating \mathcal{P} - <i>episode</i> : dark energy ρ_Λ converting into matter ρ_M	17
7.1.1	High efficiency of dark energy converting into matter	18
7.1.2	Threshold of massive pair mass and number for $\rho_M > \rho_\Lambda$	20
7.1.3	Minimal comoving radius $(Ha)^{-1}$ location	21
7.2	Massive pairs domination: \mathcal{M} - <i>episode</i>	22
7.3	Relativistic particles domination: \mathcal{R} - <i>episode</i> of genuine reheating	23
7.3.1	Massive and unstable pairs decay to relativistic particles	23
7.3.2	Energy densities of massive pairs and relativistic particles	25
7.3.3	Reheating temperature and entropy	26
8	Observations to fix reheating temperature and entropy	28
8.1	Reheating temperature and entropy vs tensor-to-scalar ratio $r < 0.048$	29
8.2	Genuine reheating $\rho_R \gg \rho_M \gg \rho_\Lambda$ and tensor-to-scalar ratio $r > 0$	31
9	Stable massive pairs and cold dark matter abundance	31
10	Remarks and summary	33
10.1	Some remarks	33
10.2	Summary	34
11	Acknowledgment	35
12	Appendix: Quantum pair oscillation details	35

1 Introduction

In the standard model of modern cosmology (Λ CDM), the cosmological constant Λ , dark matter, inflation, reheating and coincidence problem have been long-standing basic issues for decades. The inflation [1–7] reheating [8–17] are fundamental processes. The latter transition the Universe from the cold and massive state left by inflation to the hot Big Bang, and then the standard cosmology follows. The evolution follows the Friedman equations of cosmological Λ , matter and radiation energy densities. The cosmological Λ and massive particle origin are still mysteries. One calls them “dark energy” and “cold dark matter”. Moreover, their properties and interactions in the Universe’s evolution are also in question. Why their present values are coincidentally in the same order of magnitude?

To get an insight into these issues, people have been intensively studying the gravitational particle production in Friedman Universe for decades [19–32]. Based on the adiabatic and non-back-reaction approximation for a slowly time-varying Hubble function H , one adopted the semi-classical approaches to calculating the particle production rate. It is exponentially suppressed $e^{-M/H}$ for massive particles $M \gg H$ since the classical Universe evolution time scale $\mathcal{O}(1/H)$ is much larger than the quantum time scale $\mathcal{O}(1/M)$ of particle production. However, the non-adiabatic back-reactions of massive particle productions on the Hubble function can be large. One has to take them into account. People have made many efforts [23, 33–41] to study non-adiabatic back-reaction and understand massive particle productions without exponential suppression. To properly include the back-reaction of particle production on Universe evolution, one should separate fast components $\mathcal{O}(1/M)$ from slow components $\mathcal{O}(1/H)$ in the Friedman equation. Here, the fast components represent fluctuating gravitational and particle fields at the time scale $\mathcal{O}(1/M)$. The slow components represent slowly varying background fields and particle densities at the time scale $\mathcal{O}(1/H)$.

In Ref. [41], we assume the inflation epoch starts when the dark-energy density $\rho_\Lambda = \Lambda/(8\pi G)$ is the order of the Planck scale, dominates the Hubble function $H^2 \approx 8\pi G\rho_\Lambda/3$ and the matter density is negligibly small. We study the Universe undergoes a Λ -driven inflation that slowly slows down to its end by producing heavy particles of mass $M \gg H$. Inflation is a semi-classical dynamics of the time scale $\mathcal{O}(1/H)$, while massive particle production is a quantum-field dynamics of the time scale $\mathcal{O}(1/M)$. We investigate how the massive particle production density ρ_M^H back reacts ρ_Λ by separating the fast and slow components in the Friedman equation. Analysis shows H and ρ_Λ slowly decrease, as ρ_M^H slowly increases in time, namely, ρ_Λ slowly converts to ρ_M^H . It gives the quasi-de Sitter phase (slow-rolling dynamics) for inflation. The final results are consistent with observations. Here we turn to discuss the reheating epoch and possibly explain reheating energy and entropy, as well as cold dark matter, in comparison with current observations.

We review the previous results of the fast and slow components’ separation in Sec. 2, quantum massive pair production and oscillation in Sec. 3, and a massive pair plasma state in Sec. 4. We present in Secs. 5 and 6 the new studies of a complete set of differential equations and initial conditions for the reheating epoch. We numerically

solve these equations and compare the results with observations in Secs. 7 and 8. We present preliminary discussions on stable massive as cold dark matter candidate in Sec. 9. $G = M_{\text{pl}}^{-2}$ is the Newton constant, M_{pl} is the Planck scale and reduced Planck scale $m_{\text{pl}} \equiv (8\pi)^{-1/2} M_{\text{pl}} = 2.43 \times 10^{18} \text{GeV}$.

2 Slow adiabatic and fast non-adiabatic components

We discuss such fast and slow separation in the $\tilde{\Lambda}$ CDM scenario, where a time-varying cosmological $\tilde{\Lambda}$ term in the Friedman equation represents such interacting dark energy. The Friedman equations for a flat Universe are [18]

$$H^2 = \frac{8\pi G}{3}\rho; \quad \dot{H} = -\frac{8\pi G}{2}(\rho + p), \quad (2.1)$$

where energy density $\rho \equiv \rho_M + \rho_R + \rho_\Lambda$ and pressure $p \equiv p_M + p_R + p_\Lambda$. The second Equation of (2.1) is the generalised conservation law (Bianchi identity) for including time-varying cosmological term $\rho_\Lambda(t) \equiv \tilde{\Lambda}/(8\pi G)$. It reduces to the usual Equation $\dot{\rho}_M + (1 + \omega_M)H\rho_M + \dot{\rho}_R + (1 + \omega_R)H\rho_R = 0$ for time-constant ρ_Λ . The second Equation of (2.1) shows that $\dot{H} < 0$ and H decreases in time, due to the matter's gravitational attractive nature.

Separating fast components from slow ones [37], we describe the slow and fast components' decomposition: scale factor $a = a_{\text{slow}} + a_{\text{fast}}$, Hubble function $H = H_{\text{slow}} + H_{\text{fast}}$, cosmological $\tilde{\Lambda}$ and matter densities $\rho_{\Lambda, M, R} = \rho_{\Lambda, M, R}^{\text{slow}} + \rho_{\Lambda, M, R}^{\text{fast}}$ and pressures $p_{\Lambda, M, R} = p_{\Lambda, M, R}^{\text{slow}} + p_{\Lambda, M, R}^{\text{fast}}$. The fast components vary faster in time, but their amplitudes are much smaller than the slow ones. According to the order of small ratio λ of fast and slow components, the Friedman equations (2.1) decompose into two sets. The slow components $\mathcal{O}(\lambda^0)$ obey the same equations as usual Friedman equations ("macroscopic" $\mathcal{O}(H_{\text{slow}}^{-1})$ equations)

$$H_{\text{slow}}^2 = \frac{8\pi G}{3}(\rho_M^{\text{slow}} + \rho_R^{\text{slow}} + \rho_\Lambda^{\text{slow}}); \quad (2.2)$$

$$\dot{H}_{\text{slow}} \approx -\frac{8\pi G}{2}(\rho_M^{\text{slow}} + p_M^{\text{slow}} + \rho_R^{\text{slow}} + p_R^{\text{slow}}), \quad (2.3)$$

where $H_{\text{slow}} = \dot{a}_{\text{slow}}/a \approx \dot{a}_{\text{slow}}/a_{\text{slow}}$, time derivatives \dot{H}_{slow} and \dot{a}_{slow} relate to the macroscopic "slow" time variation scale $\mathcal{O}(1/H)$. The Equation of the state is $p_{R, M}^{\text{slow}} = \omega_{R, M}\rho_{R, M}^{\text{slow}}$ for normal radiation and matter (including dark matter) components. They enter the usual dynamics of Universe evolution, i.e., inflation, reheating and standard cosmology. The faster components $\mathcal{O}(\lambda^1)$ obey "microscopic" $\mathcal{O}(M^{-1})$ equations ¹,

$$H_{\text{fast}} = \frac{8\pi G}{2 \times 3H_{\text{slow}}}(\rho_M^{\text{fast}} + \rho_R^{\text{fast}} + \rho_\Lambda^{\text{fast}}); \quad (2.4)$$

$$\dot{H}_{\text{fast}} \approx -\frac{8\pi G}{2}(\rho_M^{\text{fast}} + p_M^{\text{fast}} + \rho_R^{\text{fast}} + p_R^{\text{fast}}), \quad (2.5)$$

¹They differ from the equations obtained by scalar field and potential model in Ref [37]

where the fast components of matter density ρ_M^{fast} and pressure p_M^{fast} are due to the non-adiabatic production of massive particle and antiparticle pairs in fast time variation $H_{\text{fast}} = \dot{a}_{\text{fast}}/a_{\text{slow}}$ and its time derivative \dot{H}_{fast} . They relate to the microscopic “fast” time variation scale $\mathcal{O}(1/M)$. Whereas all slow components approximate as constants “background” in “fast” time variation. The dark-energy equation of state $p_\Lambda = -\rho_\Lambda$ splits into $p_\Lambda^{\text{slow}} = \omega_\Lambda \rho_\Lambda^{\text{slow}} \mathcal{O}(\lambda^0)$ and $p_\Lambda^{\text{fast}} = \omega_\Lambda \rho_\Lambda^{\text{fast}} \mathcal{O}(\lambda^1)$, and ω_Λ is at the leading order $\mathcal{O}(\lambda^0)$. Approximation sign “ \approx ” in Eqs. (2.3,2.5) indicates we use $\omega_\Lambda \approx -1$ ².

The fast and slow components’ separation and coupled Equations (2.2-2.5) are formal and generic. It applies to all Universe’s evolution epochs: inflation, reheating and standard cosmology. However, the fast components (2.4,2.5) depend on the slow components (2.2,2.3) in different evolution epoch. In due course, we will discuss what the fast components ρ_M^{fast} and p_M^{fast} in Eqs. (2.4) and (2.5) are, and how they interact and contribute to the slow components in Friedman equations (2.2) and (2.3).

3 Quantum massive pair production and oscillation

3.1 Quantum massive pair production

In this section, we briefly discuss the Parker and Fulling results [23] for the gravitational production of a large number of massive particles ($M \gg H_{\text{slow}}$) via non-adiabatic processes. We will re-derive the results in the $\tilde{\Lambda}$ CDM (2.1) and use them for the fast components of matter density ρ_M^{fast} and pressure p_M^{fast} in Eq. (2.4,2.5).

In Ref. [23], authors discussed the results for boson fields. It is also valid for fermion fields. A quantised massive scalar matter field inside the Hubble sphere volume $V \sim H_{\text{slow}}^{-3}$ of Friedman Universe reads

$$\Phi(\mathbf{x}, t) = \sum_n A_n Y_n(\mathbf{x}) \psi_n(t). \quad (3.1)$$

Here we consider a massive field $M \gg H_{\text{slow}}$ and its modes well localise inside the horizon. The field exponentially vanishes outside the horizon H_{slow}^{-1} , i.e., the particle horizon $(a_{\text{slow}} H_{\text{slow}})^{-1}$ of comoving Hubble radius. The symbol “ n ” labels quantum states of physical wave vectors k_n , $n = 0$ and $k_0 = 0$ for the ground state³. The A_n and A_n^\dagger are time-independent annihilation and creation operators satisfying the commutation relation $[A_n^\dagger, A_n] = \delta_{n,n'}$. The time-separate equation for $\psi_n(t)$ is

$$\partial_t^2 \psi_n(t) + \omega_n(t)^2 \psi_n(t) = 0, \quad \omega_n(t)^2 = k_n^2 + M^2, \quad (3.2)$$

²Here, $\omega_\Lambda \approx -1$ is due to time-varying $\tilde{\Lambda}$ dark energy interacting with matter [42]. In contrast, $\omega_\Lambda = -1$ in non-interacting constant Λ case.

³In Ref. [23], the principal quantum number n is the angular momentum number “ $\ell = 0, 1, 2, \dots$ ” and $Y_n(\mathbf{x}) = Y_{\ell,m}(\mathbf{x})$ are the four-dimensional spherical harmonics for the closed Robertson-Walker metric and $\Lambda = 0$. The ground state is $n = \ell = 0$. Here we discuss the case of a flat Robertson-Walker metric and $\Lambda \neq 0$, for which a massive scalar matter field has no discrete spectra. However, this is not important here since we adopt the Parker-Fulling result (3.6) for the ground state $k_0 = 0$ and $\omega_0 = M$, which well localizes inside the horizon.

and Wronskian-type condition $\psi_n(t)\partial_t\psi_n^*(t) - \psi_n^*(t)\partial_t\psi_n(t) = i$ in the conformal coupling case. Expressing

$$\psi_n(t) = \frac{1}{(2V\omega_n)^{1/2}} \left(\alpha_n^*(t)e^{-i\int^t\omega_n dt} + \beta_n^*(t)e^{i\int^t\omega_n dt} \right) \quad (3.3)$$

in terms of $\alpha_n(t)$ and $\beta_n(t)$, Equation (3.2) becomes

$$\begin{aligned} \partial_t\alpha_n(t) &= C_n e^{-2i\int^t\omega_n dt}\beta_n(t); \\ \partial_t\beta_n(t) &= C_n e^{2i\int^t\omega_n dt}\alpha_n(t), \end{aligned} \quad (3.4)$$

and $|\alpha_n|^2 - |\beta_n|^2 = 1$, where $C_n \equiv 3H\omega_n^{-2}[k_n^2/3 + M^2/2]$. In an adiabatic process for slowly time-varying $H = H_{\text{slow}}$, the particle state $\alpha_n(0) = 1$ and $\beta_n(0) = 0$ evolves to $|\alpha_n(t)| \gtrsim 1$ and $|\beta_n(t)| \neq 0$. Positive and negative frequency modes get mixed, leading to particle productions of probability $|\beta_n(t)|^2 \propto e^{-M/H_{\text{slow}}}$.

We will study particle production in non-adiabatic processes of rapidly time-varying H_{fast} , α_n and β_n . We focus only on the ground state $n = 0$ of the lowest-lying massive mode $M \gg H$. First, we recall that Parker and Fulling introduced transformation [23],

$$A_0 = \gamma^* B + \delta B^\dagger, \quad B = \delta A_0^\dagger - \gamma A_0, \quad (3.5)$$

$[B, B^\dagger] = 1$, and two mixing constants obey $|\gamma|^2 - |\delta|^2 = 1$. For a given A_n and its Fock space, the state $|\mathcal{N}_{\text{pair}}\rangle$ is defined by the conditions $A_{n \neq 0}|\mathcal{N}_{\text{pair}}\rangle = 0$ and

$$B^\dagger B|\mathcal{N}_{\text{pair}}\rangle = \mathcal{N}_{\text{pair}}|\mathcal{N}_{\text{pair}}\rangle, \quad \mathcal{N}_{\text{pair}} \gg 1. \quad (3.6)$$

The B^\dagger and B are time-independent creation and annihilation operators of the pair of mixed positive frequency A_0 particles and negative frequency A_0^\dagger antiparticle. The state $|\mathcal{N}_{\text{pair}}\rangle$ contains $\mathcal{N}_{\text{pair}} = 1, 2, 3, \dots$ pairs, and it is the ground state of non-adiabatic interacting system of fast varying H_{fast} and massive pair production and annihilation. It is a coherent superposition of states of a large occupation number $\mathcal{N}_{\text{pair}}$ of particle and anti-particle pairs. In Ref. [23], the authors compared it with the BCS condensate state in superconductivity theory and contrasted it with the normal single-particle state. In this coherent condensate state $|\mathcal{N}_{\text{pair}}\rangle$ and $\mathcal{N}_{\text{pair}} \gg 1$, neglecting higher mode $n \neq 0$ contributions, they obtained the negative quantum pressure and positive quantum density of coherent pair field, see Eqs. (59) and (60) of Ref. [23],

$$\begin{aligned} p_M^{\text{fast}} &= -\frac{M(2\mathcal{N}_{\text{pair}} + 1)}{2\pi^2 V} \left\{ \text{Re}[\gamma^* \delta (|\alpha|^2 + |\beta|^2)] \right. \\ &\quad \left. + (2|\delta|^2 + 1)\text{Re}(\alpha^* \beta e^{2iMt}) \right\}, \end{aligned} \quad (3.7)$$

$$\begin{aligned} \rho_M^{\text{fast}} &= \frac{M(2\mathcal{N}_{\text{pair}} + 1)}{\pi^2 V} \left\{ \text{Re}[\gamma \delta^* \alpha \beta] \right. \\ &\quad \left. + (|\delta|^2 + 1/2)(|\beta|^2 + 1/2) \right\}, \end{aligned} \quad (3.8)$$

where $\omega_{n=0} = M$, $\alpha_{n=0} = \alpha$ and $\beta_{n=0} = \beta$. They satisfy the continuity equation of energy-momentum conservation. In addition to non-vanishing $|\beta|^2 \neq 0$, the large occupation number $\mathcal{N}_{\text{pair}} \gg 1$ in the coherent state (3.6) is crucial for the significant gravitational production of massive pairs. It differs from adiabatic particle production in the vacuum state of zero particles. For a closed Universe case, they adopted the pressure (3.7) and density (3.8) for studying the avoidance of cosmic singularity at the beginning of the Universe. In their sequent article [43], the authors confirm Eqs. (3.7) and (3.8) by studying the regularisation of higher mode contributions to the energy-momentum tensor of a massive quantized field of closed, flat, and hyperbolic spatial spaces. In the case of heavy particles produced near the Planck scale, the renormalization of high-energy contributions should not be the same as the case of produced light particles in low energies [39]. The natures of the massive coherent pair state $|\mathcal{N}_{\text{pair}}\rangle$ (3.6) of the pressure (3.7) and density (3.8) are rather generic for non-adiabatic production of massive particles in curved spacetime. The coherent state $|\mathcal{N}_{\text{pair}}\rangle$ (3.6) and (3.7,3.8) should be valid also for $M \gtrsim H$, provided the pair occupation number $\mathcal{N}_{\text{pair}} \gg 1$. Note that p_M^{fast} (3.7) and ρ_M^{fast} (3.8) represent the quantum pressure and density of massive coherent pair state (3.6) in short quantum time scales $\mathcal{O}(1/M)$. They do not follow the usual equation of the state of classical matter.

To end this section, we emphasize two points. (i) The quantum pressure p_M^{fast} (3.7) oscillates, and its value can be positive or negative in oscillations of frequency $1/M$, depending on modes' equation (3.4), superposition coefficients γ, δ (3.5) and mass M values. The negative value of microscopic time-averaged quantum pressure p_M^{fast} is crucial for forming the coherent condensate state $|\mathcal{N}_{\text{pair}}\rangle$ (3.6) of a large occupation number $\mathcal{N}_{\text{pair}}$ of massive particle and anti-particle pairs produced. (ii) Such coherent condensate state $|\mathcal{N}_{\text{pair}}\rangle$ occurs only at the ground state $k_0 = 0$ and $n = 0$, i.e., the state of $\ell = 0$ spherical S -wave. For high angular momentum states $\ell \neq 0$, the time-averaged pressure becomes non-negative classical values $\propto \ell(\ell + 1)$ [23]. Therefore, the coherent condensate state $|\mathcal{N}_{\text{pair}}\rangle$ cannot form for high-energy states $\ell \neq 0$. It gives us a lesson that the high-energy modes' renormalization or subtraction prescription for massive particles ($M \sim M_{\text{pl}} \gg H$) production is not the same as light particles ($M \ll H \ll M_{\text{pl}}$) production.

3.2 Quantum massive pair oscillation

Following their approach for the ground state $k_n = 0$, we arrive at the same quantum pressure (3.7) and density (3.8) in the Λ CDM. In our case, we consider the state (3.6) as a coherent condensate state of very massive $M \gg H_{\text{slow}}$ and large number $\mathcal{N}_{\text{pair}} \gg 1$ pairs. Therefore, $M(2\mathcal{N}_{\text{pair}} + 1)$ in Eqs. (3.7,3.8) can be larger than the Planck mass, and higher mode ($k_n \neq 0, n \neq 0$) contributions can be neglected. Their regularisation and corrections will be studied in future. In this article, we adopt p_M^{fast} (3.7) and ρ_M^{fast} (3.8) as the fast components in Eqs. (2.4,2.5) to find their non-adiabatic back-reactions on fast components H_{fast} and $\rho_{\Lambda}^{\text{fast}}$.

We will study the reheating epoch when the Hubble scale and pair mass are very much smaller than the Planck scale, i.e., $H_{\text{slow}} < M \ll m_{\text{pl}}$ and $\mathcal{N}_{\text{pair}} \gg 1$. Therefore, in the unit of the mass M and the critical density $\rho_{\text{crit}} = 3m_{\text{pl}}^2 H_{\text{slow}}^2$, we express the

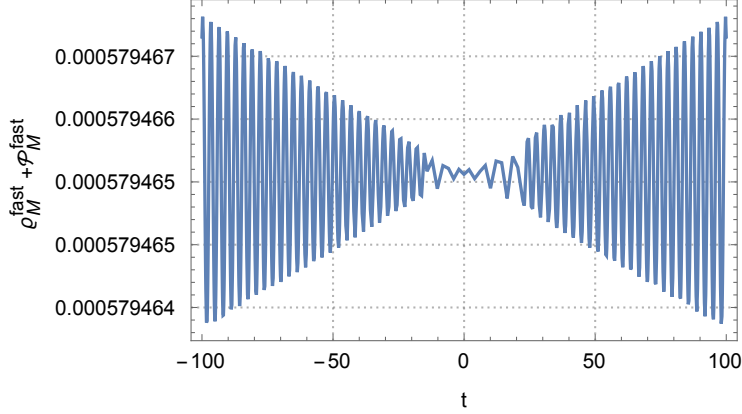


Figure 1. We show the quantum pair density and pressure oscillations in microscopic time t in the unit of M^{-1} , by using $H_{\text{slow}}/M \approx 10^{-3}$, $M \simeq 10^{-5}m_{\text{pl}}$, $\mathcal{N}_{\text{pair}} \simeq 10^{12}$ and $\delta = 1$, with $C_0 = (3/2)h_{\text{fast}}(H_{\text{slow}}/M)$ and verified condition $|\alpha|^2 - |\beta|^2 = 1$. It shows that a large number of massive pairs creates significantly oscillating quantum pressure $\mathcal{P}_M^{\text{fast}}$ (3.9) and ϱ_M^{fast} (3.10) in the unit of ρ_{crit} , the oscillating amplitudes $\delta\varrho_M^{\text{fast}}/\varrho_M^{\text{fast}}$ and $\delta\mathcal{P}_M^{\text{fast}}/\mathcal{P}_M^{\text{fast}}$ are about $\mathcal{O}(10^{-3})$. For a long time, the coherent oscillations approach stable configurations in time. For more details and figures, for instance, the fast components $\varrho_\Lambda^{\text{fast}}$, h_{fast} and \dot{h}_{fast} , see Fig. 11 in Appendix. Note that the pair number $\mathcal{N}_{\text{pair}}$, mass scales \bar{M} and H_{slow} values differ from those used for inflation see Fig. 1 in Ref. [41].

dimensionless quantum pressure (3.7) and density (3.8) as ⁴

$$\mathcal{P}_M^{\text{fast}} = -\frac{\bar{M}H_{\text{slow}}}{6\pi^2m_{\text{pl}}}\left\{\text{Re}[\gamma^*\delta(|\alpha|^2 + |\beta|^2)] + (2|\delta|^2 + 1)\text{Re}(\alpha^*\beta e^{2iMt})\right\}, \quad (3.9)$$

$$\varrho_M^{\text{fast}} = +\frac{\bar{M}H_{\text{slow}}}{3\pi^2m_{\text{pl}}}\left\{\text{Re}[\gamma\delta^*\alpha\beta] + (|\delta|^2 + 1/2)(|\beta|^2 + 1/2)\right\}, \quad (3.10)$$

where $\bar{M} \equiv (2\mathcal{N}_{\text{pair}} + 1)(M/m_{\text{pl}})$. The fast component equations (2.4,2.5) become,

$$\begin{aligned} h_{\text{fast}} &= \frac{1}{2}(\varrho_M^{\text{fast}} + \varrho_\Lambda^{\text{fast}}); \\ \dot{h}_{\text{fast}} &= -\frac{3}{2}(\varrho_M^{\text{fast}} + \mathcal{P}_M^{\text{fast}}), \end{aligned} \quad (3.11)$$

where $h_{\text{fast}} \equiv H_{\text{fast}}/H_{\text{slow}}$ and $\varrho_\Lambda^{\text{fast}} \equiv \rho_\Lambda^{\text{fast}}/\rho_{\text{crit}}$. Here we only consider the fast components of massive particle productions and oscillations inside the Horizon and neglect the fast components of light particles.

Using negative $\mathcal{P}_M^{\text{fast}}$ (3.9) and positive definite ϱ_M^{fast} (3.10), we search for a solution of fast component equation (3.11) and quantum fluctuating mode equations (3.4) in the period $[-t, t]$ of the microscopic time $t \sim H_{\text{fast}}^{-1}$. The period is around the macroscopic time $t_{\text{slow}} \sim H_{\text{slow}}^{-1}$, when the slow components a_{slow} , H_{slow} , $\rho_{M,\Lambda}^{\text{slow}}$ and $p_{M,\Lambda}^{\text{slow}}$ are determined by the Friedman equations (2.2,2.3). The integrals $\int^t \omega_n dt$ are over the microscopic

⁴In the previous article [41], we use the reduce Planck mass m_{pl} and energy density m_{pl}^4 as the unit for studying inflation.

time t characterised by the time scale $1/M$. Its lower limit is $t = 0$ by setting $t_{\text{slow}} = 0$ as a reference time, when $a_{\text{fast}}(0) = 0$,

$$H_{\text{fast}}(0) = \dot{a}_{\text{fast}}/a_{\text{slow}} = 0; \quad \alpha(0) = 1, \quad \beta(0) = 0. \quad (3.12)$$

The real value $\gamma^*\delta$ condition in Eqs. (3.9), (3.10) leads to the time symmetry: $a^{\text{fast}}(t) = a^{\text{fast}}(-t)$, $\alpha(t) = \alpha^*(-t)$ and $\beta(t) = \beta^*(-t)$ [23]. When $t \leftrightarrow -t$, positive and negative frequency modes interchange. Here we use $a_{\text{slow}} \neq 0$, $H_{\text{slow}} \neq 0$ and co-moving radius $(Ha)^{-1} \approx (H_{\text{slow}}a_{\text{slow}})^{-1}$ of Hubble volume $V \sim H_{\text{slow}}^{-3}$.

In microscopic time t of unit M^{-1} , we numerically solve non-linearly coupled Eqs. (3.4) and (3.9-3.11) with the initial condition (3.12). We report the results in Fig. 1 and details in Fig. 11 of Appendix. Similar to the previous results [41], we find that in the quantum period of microscopic time t , the negative quantum pressure $\mathcal{P}_M^{\text{fast}} < 0$ and back-reaction effects lead to the *quantum pair oscillation* in a time characterised by the frequency $\omega \sim M$. The small $a_{\text{fast}}(t)$ varies around a_{slow} at $t_{\text{slow}} \equiv 0$. The massive pairs' density and pressure $(\varrho_M^{\text{fast}}, \mathcal{P}_M^{\text{fast}})$ oscillate coherently with the spacetime fields $(h_{\text{fast}}, \dot{h}_{\text{fast}}, \varrho_\Lambda^{\text{fast}})$ oscillations. Their oscillatory structures imply a quantum back-and-forth process in microscopic time scale $\mathcal{O}(1/M)$

$$\mathcal{S} \Leftrightarrow \bar{F}F \quad (3.13)$$

between spacetime fields $\mathcal{S}(h_{\text{fast}}, \dot{h}_{\text{fast}}, \varrho_\Lambda^{\text{fast}})$ and massive particle pairs $\bar{F}F(\varrho_M^{\text{fast}}, \mathcal{P}_M^{\text{fast}})$, previously discussed [39]. These results show the highly non-adiabatic and complex nature of massive pair-production processes and collective oscillations. Attributed to complex back-and-forth reactions at the scale $\mathcal{O}(1/M)$, the quantum massive pair oscillation (3.13) cannot be described by oscillating scalar fields with polynomial potential.

As shown in Figs. 1 and 11, for the microscopic time $t \gg 1/M$, the positive quantum pair density $\varrho_M^{\text{fast}} > 0$ indicates particle creations without $e^{-M/H}$ suppression. It is consistent with increasing Bogoliubov coefficient $|\beta(t)|^2$ that mixes positive and negative energy modes. Observe that $\varrho_M^{\text{fast}} > |\mathcal{P}_M^{\text{fast}}|$ and the sum $\varrho_M^{\text{fast}} + \mathcal{P}_M^{\text{fast}} > 0$ is positive definite, leading to the decreasing $h_{\text{fast}}(t)$ (3.11). As a consequence, for positive time ($t > 0$) increasing (forward the future), the fast components h_{fast} and $\varrho_\Lambda^{\text{fast}}$ decrease, in order for pair production. Whereas for negative time ($t < 0$) increasing (backward the past), h_{fast} and $\varrho_\Lambda^{\text{fast}}$ increases, due to pair annihilation. In both situations, the $\rho_\Lambda^{\text{fast}}$ is negative and ρ_M^{fast} is positive, as required by the energy conservation (3.11) in the massive pairs' production via fast oscillating h_{fast} and \dot{h}_{fast} . Equations $\rho_{\Lambda, M} = \rho_{\Lambda, M}^{\text{slow}} + \rho_{\Lambda, M}^{\text{fast}}$ imply the dark energy ρ_Λ decreases and matter ρ_M increases, where the slow components $\rho_{\Lambda, M}^{\text{slow}}$ are fixed values at $t = t_{\text{slow}} \equiv 0$. In this sense, dark energy converts to massive pairs (matter) in a microscopic time scale, whereas the case for a macroscopic time scale will be studied in Sec. 5. It is our finding that the energy density and pressure (3.9, 3.10) of the condensate state $|\mathcal{N}_{\text{pair}}\rangle$ coherently interacts and exchanges energy with the fast components of spacetime variation (3.11). Such the back-and-forth reaction at the scale $1/M$ was not studied in Ref. [23] for the $|\mathcal{N}_{\text{pair}}\rangle$ condensate state's energy density (3.8) and pressure (3.7). In our solutions, we find the quantum pressure $\mathcal{P}_M^{\text{fast}}$ and its time average are negative see Fig. 11 in Appendix.

It implies the possibility that the condensate state $|\mathcal{N}_{\text{pair}}\rangle$ retains while it coherently interacts with the fast components of spacetime horizon variation (3.13).

This phenomenon is dynamically analogous to the plasma oscillation of electron-positron pair production in an external alternating electric field E [44]. The pair production rate is not exponentially suppressed by $e^{-\pi M^2/E}$ [45]. The coherent plasma state of electron-positron pairs is analogous to the coherent pair state $|\mathcal{N}_{\text{pair}}\rangle$ (3.6) and quantum pair oscillation, shown in Fig. 1.

Such massive and semi-classical state of large occupation number (3.6) and quantum pair oscillation (Fig. 1) well localises inside the horizon. They persist throughout the entire Universe's history, independent of slow components H_{slow} and $\rho_{\Lambda, M, R}^{\text{slow}}$ values in Friedman equations (2.2, 2.3). However, the pair mass M (oscillating frequency $\omega \approx M$) and pair number $\mathcal{N}_{\text{pair}}$ depend on slow components' values in the Friedman equations (2.2, 2.3). It is necessary and deserves to proceed with further studies.

4 Massive pair plasma state and holographic hypothesis

4.1 Reasons for a macroscopic description

We see the non-adiabatic and back-reacting phenomena of massive pairs' production and oscillation at a time scale $\mathcal{O}(1/M)$. How the fast oscillating components $\mathcal{P}_M^{\text{fast}}$ (3.9) and ϱ_M^{fast} (3.10) in Eqs. (2.4, 2.5) couple to the slow components in Friedman equations (2.2, 2.3). It is a difficult task to simultaneously analyze $\mathcal{O}(1/M)$ and $\mathcal{O}(1/H)$ back-reaction dynamics even numerically since two scales $M \gg H$ are very different. To deal with this difficulty, we adopt two approximate steps. First, due to nontrivial time-averaged values of fast components over the microscopic time $t \gg 1/M$, we assume the massive pair production and oscillation form a *massive pair plasma state* in the macroscopic time scale. We model such a semi-classical state as a perfect fluid by defining the effective density and pressure. Second, we discuss how it back-and-forth interacts and contributes to the slow components in the Friedman equations.

Figure 1 shows that massive pair quantum pressure $\mathcal{P}_M^{\text{fast}}$ (3.9) and density ϱ_M^{fast} (3.9) rapidly oscillate with the fast components h_{fast} and $\varrho_{\Lambda}^{\text{fast}}$ (3.11) in microscopic time. Their oscillating amplitudes are significantly large and not dampening in time. It, therefore, expects to form a *massive pair plasma state* in a macroscopic time and space. However, to study its effective impacts on the classical Friedman equations (2.3), we have to discuss two problems stemming from the scale difference $M \gg H_{\text{slow}}$.

- (i) First, the different time scales. It is impossible to even numerically integrate slow and fast component coupled equations (2.3, 2.5) due to their vastly different time scales. On this aspect, we consider the fast-component averages $\langle \dots \rangle$ over the microscopic time scale. Figure 1 shows $\varrho_M^{\text{fast}} + \mathcal{P}_M^{\text{fast}} > 0$, which does not oscillate alternatively between negative and positive values. Its time average $\langle \varrho_M^{\text{fast}} + \mathcal{P}_M^{\text{fast}} \rangle$ does not vanish. Other fast-component averages do not vanish as well. Fast-component averages have another time scale τ_M (5.1) in response to the slow horizon variations H_{slow} in macroscopic time. It is a kind of “relaxation”

time scale and differs from the oscillating one $1/M$. Therefore, in principle, fast-component averages possibly affect the Friedman equation at the macroscopic time scale. In practice, the appropriate modelling of fast-component averages can avoid the difficulty of vastly different scale dynamics in calculations, and the scenario becomes tractable. However, we have to check its self-consistency with observation.

- (ii) Second, the spatial distribution. We do not know the spatial distribution of the massive pair condensate state $|\mathcal{N}_{\text{pair}}\rangle$. Namely, we do not know the radial dependence of the quantum pressure and density (3.7,3.8) or (3.9,3.10), since the Ref. [23] authors obtained them by using the vacuum expectation value of field $\Phi(\mathbf{x}, t)$ (3.1) energy-momentum tensor integrated over the entire space. There, they studied the cosmic singularity problem in the Universe beginning $M \gtrsim H$ case, namely the massive mode wavelength M^{-1} is comparable with the horizon size H^{-1} . Here, we study the case $M \gg H \approx H_{\text{slow}}$, namely the massive mode wavelength M^{-1} is much smaller than the horizon size H_{slow}^{-1} . As a hypothesis, we speculate that the massive pair condensate state $|\mathcal{N}_{\text{pair}}\rangle$ and the coherent oscillation (3.13) with H_{fast} and \dot{H}_{fast} spatially localize nearby the horizon following the holographic principle [46–48]. The arguments are the following. (a) Such condensate state $|\mathcal{N}_{\text{pair}}\rangle$ and oscillation (3.13) collectively couple with the fast components H_{fast} and \dot{H}_{fast} , which are quantum modes at short wavelengths ($1/M$). These modes should associate with the horizon surface according to the holographic principle. (b) The massive pair condensate state $|\mathcal{N}_{\text{pair}}\rangle$ is a ground state of a spherically symmetric S wave. (c) Such a very massive state of the radial size about $M^{-1} \ll H_{\text{slow}}^{-1}$ is inside the horizon H_{slow}^{-1} of the Friedman Universe, whose isotropic homogeneity extends up to the horizon.

Based on these hypotheses, we will introduce a holographic and massive pair plasma state that gives an effective description of the condensate state $|\mathcal{N}_{\text{pair}}\rangle$ and coherent oscillation (3.13) at macroscopic space and time scales.

4.2 Effective description of a massive pair plasma state

Based on these considerations, we assume a massive pair plasma state forms in a macroscopic time scale. We describe such macroscopic state as a perfect fluid state of effective number n_M^H and energy ρ_M^H densities ⁵

$$\rho_M^H \equiv 2\chi m^2 H_{\text{slow}}^2, \quad n_M^H \equiv \chi m H_{\text{slow}}^2; \quad m^2 \equiv \sum_f g_d^f M_f^2, \quad (4.1)$$

and pressure $p_M^H = \omega_M^H \rho_M^H$. The $\omega_M^H \approx 0$ for $m \gg H_{\text{slow}}$ and its upper limit is $1/3$. The introduced mass parameter m represents possible particle masses M_f , degeneracies g_d^f and the mixing coefficient δ (3.5). The degeneracies g_d^f plays the same role of pair number $\mathcal{N}_{\text{pair}}$ in Eqs. (3.7,3.8) or (3.9,3.10). The pair masses M_f are smaller

⁵Here we present the simplest state, and it can be a more complex state of massive pair plasma.

than the Planck mass M_{pl} , but the mass parameter m can be larger than M_{pl} for a large occupation number $\mathcal{N}_{\text{pair}} \gg 1$ or degeneracy $g_d^f \gg 1$. Note that the massive pair plasma state contains (i) unstable massive pairs that couple and decay to light particles; (ii) stable massive pairs with gravitational interaction only. Besides, one should differ the massive pair plasma state density ρ_M^H (4.1) from the normal matter or radiation (including dark matter) density $\rho_{M,R} \propto (1/a)^{3(1+\omega_{M,R})}$. The reason is that the massive pair plasma state (4.1) attributes to quantum pair production and oscillation, which couple to the oscillating spacetime fields $\mathcal{S}(h_{\text{fast}}, \dot{h}_{\text{fast}}, \varrho_{\Lambda}^{\text{fast}})$ of Hubble function and dark energy. To some extent, we may consider the massive pair plasma state as an “equilibrium state” between quantum massive pairs and spacetime field oscillations.

Following the previous subsection discussions, we explain the reasons why the densities (4.1) are proportional to $\chi m H_{\text{slow}}^2$, rather than H_{slow}^3 of the entire Hubble volume V . The “surface area” factor H_{slow}^2 is attributed to the spherical symmetry of Hubble volume. The “radial size” factor χm is the layer width λ_m introduced as an effective parameter to describe the properties: (i) for $m \gg H_{\text{slow}}$ the massive pair plasma state localizes as a spherical layer near to the horizon; (ii) the layer radial width $\lambda_m < H_{\text{slow}}^{-1}$ depends on the massive pair plasma oscillation dynamics⁶, rather than the H_{slow} dynamics govern by the Friedman equations (2.3). The width parameter χ expresses the layer width $\lambda_m = (\chi m)^{-1} \gg 1/m$,

$$\lambda_m = (\chi m)^{-1} < H_{\text{slow}}^{-1}, \quad 1 \gg \chi > (H_{\text{slow}}/m). \quad (4.2)$$

Note that studying the prescription of high-energy modes’ subtraction for $m \gg H$, we approximately obtained the mean density $n_M^H \approx \chi m H^2$ (4.1) and $\chi \approx 1.85 \times 10^{-3}$ by studying massive fermion pair productions in a De Sitter spacetime of constant H and scaling factor $a(t) = e^{iHt}$ [39, 40]. We adopt this χ value for numerical calculations in the present article.

Since the parameters m and χm represent time-averaged values over fast time oscillations of massive pair plasma state, we consider m and χm as approximate constants in slowly varying macroscopic time for the Friedman equations. However, the typical m and χm values should be different for Universe evolution epochs since the fast-component equations for massive pair productions and oscillations depend on the H_{slow} value, see Sec. 3. We used the parameter m^* for inflation, \hat{m} for reheating and m_M for the epochs after reheating. We will fix these parameter values by observations.

To end this section, we have to point out that (i) the pressure p_M^H and density ρ_M^H (4.1) are effective descriptions of the massive pair plasma state in macroscopic scales, that result from the coherence condensation state (3.6,3.7,3.8) and oscillating dynamics (Fig. 1) in microscopic scales; (ii) they contribute to the “slow” components ρ_M^{slow} and p_M^{slow} in the “macroscopic” $\mathcal{O}(H_{\text{slow}}^{-1})$ Friedman equations (2.2,2.3). It means that in the Friedman equations (2.2,2.3), the matter density and pressure terms ρ_M^{slow} and p_M^{slow} contain (a) the normal matter state contributions and (b) the massive pair plasma state contributions. This will be clarified in the next Section. We shall study the massive pair plasma state effects on each epoch of the Universe’s evolution. Here we investigate its impact on reheating.

⁶It may also include self-gravitating dynamics due to the pair plasma state being very massive.

After we adopt the effective description of massive pair plasma state (4.1), the quantum massive pair oscillation (Fig. 1) of fast components ($\varrho_M^{\text{fast}}, \mathcal{P}_M^{\text{fast}}, h_{\text{fast}}, \dot{h}_{\text{fast}}, \varrho_\Lambda^{\text{fast}}$) and $p_\Lambda^{\text{fast}} \approx -\rho_\Lambda^{\text{fast}}$ details at the scale $\mathcal{O}(1/M)$ average out and become irrelevant for the macroscopic scale $\mathcal{O}(\tau_H)$ and $\mathcal{O}(\tau_M)$ processes: inflation, reheating and standard cosmology. The relevant quantities and equations are massive pair plasma state $p_M^H = \omega_M^H \rho_M^H$ (4.1) and slow components obeying Friedman equations (2.2,2.3), and their interacting equation (5.5). The final results depend only on the plasma state (4.1) with the mass m and width χ parameters. Henceforth we ignore the “fast” components, sub-script, and super-scripts “slow” will be dropped.

5 Back-and-forth process and cosmic rate equation

In Sec. 3, we show massive pairs’ production and annihilation at time scale $\mathcal{O}(1/M)$ via quantum pair oscillations, and dark energy effectively converts to massive pairs for the microscopic time $t \gg 1/M$. These are the quantum back-and-forth process (3.13). By non-vanishing averages over microscopic time, these microscopic back-reaction processes should impact the classical and slow components in Friedman’s equations. Using massive pair plasma state (4.1), we will discuss how to effectively describe the back-and-forth process between massive pairs and spacetime fields (H, ρ_Λ) at a macroscopic time scale ($1/H$).

5.1 Stable massive pairs and cosmic rate equation

We discuss here how the massive pair plasma state (4.1) back-reacts and contributes to the slow components in Friedman equations. First, we introduce the mean pair production rate Γ_M to describe the massive pair plasma state variation as the macroscopic time t varies. We estimate the total number of particles produced inside the Hubble sphere $N \approx n_M^H H^{-3}/2$ and mean pair production rate w.r.t. macroscopic time variation dt ,

$$\Gamma_M = \frac{dN}{2\pi dt} \approx \frac{\chi m}{4\pi} \epsilon, \quad \tau_M^{-1} = \Gamma_M. \quad (5.1)$$

It is in terms of the parameter χm (4.2) and Universe evolution ϵ -rate defined as,

$$\epsilon \equiv -\frac{\dot{H}}{H^2} = \frac{3(1 + \omega_M)\rho_M + (1 + \omega_R)\rho_R}{2(\rho_\Lambda + \rho_M + \rho_R)}. \quad (5.2)$$

The second equation comes from the Friedman equations (2.2,2.3). The asymptotic values $\epsilon \approx 0$, $\epsilon \approx 2$ and $\epsilon \approx 3/2$ correspond to the dark-energy (inflation), radiation, and matter dominant epochs, respectively.

The massive pair plasma state ρ_M^H (4.1) effectively represents an equilibrium state of quantum pair and spacetime field oscillations (3.13). It not only depends on the Hubble function H , but also contributes to the normal matter density ρ_M . Back reactions must act on ρ_M^H , when H and ρ_M vary in time following the Friedman equations. Moreover, the massive pair plasma state variation time scale $\tau_M = \Gamma_M^{-1}$ is smaller than the normal matter density ⁷ ρ_M variation time scale $\tau_H = 1/H$. The difference $\tau_H > \tau_M$

⁷For the sake of brief notation, ρ_M stands for $\rho_{M,R}$ in this section

implies the back-and-forth interaction between the massive pair plasma state density and the normal matter density

$$\rho_M^H \Leftrightarrow \rho_M, \quad (5.3)$$

during the Universe's evolution. The process is induced by quantum pair oscillation coherently with fast oscillating components of the Hubble function and dark energy.

To model such dynamics (5.3), we recall the rate equation for the back-and-forth process $e^+e^- \Leftrightarrow \gamma\gamma$ [49–52]:

$$\frac{dn_{e^+e^-}(t)}{dt} + 3Hn_{e^+e^-}(t) = \langle\sigma v\rangle \left(n_{e^+e^-}^2|_{\text{eq}} - n_{e^+e^-}^2 \right), \quad (5.4)$$

where $n_{e^+e^-}(t)$ is the electron and positron pair density governed by the macroscopic time scale H^{-1} evolution. While $n_{e^+e^-}|_{\text{eq}}$ is the density of electrons and positrons in equilibrium with two photons $n_{\gamma\gamma}|_{\text{eq}}$ in microscopic time scale $(\langle\sigma v\rangle n_{e^+e^-})^{-1}$, namely $n_{e^+e^-}|_{\text{eq}} \approx n_{\gamma\gamma}|_{\text{eq}}$. The RHS represents the averaged interacting rate $dN/dt \approx \langle\sigma v\rangle n_{e^+e^-}$ for microscopic detail balance between $n_{e^+e^-}(t)$ and $n_{e^+e^-}|_{\text{eq}}$. They are coupled for $n_{e^+e^-}|_{\text{eq}} \approx n_{e^+e^-}$ and decoupled for $n_{e^+e^-}|_{\text{eq}} \ll n_{e^+e^-}$.

We make the following analogies: $n_{e^+e^-} \leftrightarrow \rho_M$, $n_{e^+e^-}|_{\text{eq}} \leftrightarrow \rho_M^H$ and photons $n_{\gamma\gamma}|_{\text{eq}}$ correspond to fast oscillating components of the Hubble function and dark energy. This analogy motivates us to propose an effective cosmic rate equation

$$\dot{\rho}_M + 3(1 + \omega_M)H\rho_M = \Gamma_M(\rho_M^H - \rho_M) - \Gamma_M^{\text{de}}\rho_M, \quad (5.5)$$

of the Boltzmann type for the the back-and-forth ρ_M and ρ_M^H interaction (5.3) in the Universe's evolution. It represents a general conservation law of dark energy and matter, including massive pair plasma state ρ_M^H (4.1) with the production rate (5.1). The term $3(1 + \omega_M)H\rho_M$ of the time scale $[3(1 + \omega_M)H]^{-1}$ represents the space-time expanding effect on the density ρ_M . While $\Gamma_M\rho_M^H$ is the source term and $\Gamma_M\rho_M$ is the depletion term. The detailed balance term $\Gamma_M(\rho_M^H - \rho_M)$ indicates how two densities ρ_M^H and ρ_M of different time scales couple together. The ratio $\Gamma_M/H > 1$ indicates the coupled case, and $\Gamma_M/H < 1$ indicates the decoupled case. The last term $\Gamma_M^{\text{de}}\rho_M$ represents unstable massive pairs' decay to relativistic particle pairs $\bar{\ell}\ell$, and the decay rate and time are given by

$$\Gamma_M^{\text{de}} = g_Y^2 m, \quad \tau_R = (\Gamma_M^{\text{de}})^{-1}, \quad (\bar{F}F \Rightarrow \bar{\ell}\ell) \quad (5.6)$$

where g_Y is the Yukawa coupling between the massive pairs ($\bar{F}F$) and relativistic particles. It is important to note that the decay rate Γ_M^{de} (5.6) depends not only on the Yukawa coupling g_Y but also on the phase space of final states. While for stable massive pairs, the decay rate Γ_M^{de} is zero.

The combination of cosmic rate equation (5.5) and Friedman equations (2.3) yields

$$\dot{\rho}_\Lambda = -\Gamma_M(\rho_M^H - \rho_M) + \Gamma_M^{\text{de}}\rho_M = -\delta Q, \quad (5.7)$$

$$\dot{\rho}_M + 3(1 + \omega_M)H\rho_M = \delta Q \quad (5.8)$$

where $\delta Q \equiv \Gamma_M (\rho_M^H - \rho_M) - \Gamma_M^{\text{de}} \rho_M$, representing the interaction and exchange between dark energy and normal matter via the massive pair plasma state ρ_M^H . To discuss this in some more detail, we ignore the decay term $\Gamma_M^{\text{de}} \rho_M$. It is negligible for unstable pairs, provided $\Gamma_M \gg \Gamma_M^{\text{de}}$. We point out four particular cases:

- (i) Recall the results [41] for the inflation epoch, when the ratio $\Gamma_M/H \propto \epsilon_* \ll 1$, $\rho_\Lambda \gg \rho_M^H$ and $\rho_M^H \gg \rho_M$ ⁸. Equations (5.7,5.8) become $\dot{\rho}_\Lambda \approx -\Gamma_M \rho_M^H \lesssim 0$ showing ρ_M^H production costs dark energy, but it adds into matter-energy $\dot{\rho}_M + 3(1 + \omega_M)H\rho_M \approx \Gamma_M \rho_M^H \gtrsim 0$. The exchange rate $\delta Q \approx \Gamma_M \rho_M^H \gtrsim 0$ is positive and small. It yields $\dot{\rho}_\Lambda \lesssim 0$ and $\dot{H} \lesssim 0$, i.e., slow-rolling dynamics for inflation. Dark energy converts slowly to matter till inflation ends when $\Gamma_M/H \approx 1$.
- (ii) In a short pre-reheating episode, when $\Gamma_M/H \gg 1$ and $\rho_\Lambda > \rho_M^H > \rho_M$, the exchange rate $\delta Q \gg 1$ is large. Dark energy rapidly converts to matter till $\rho_M^H \approx \rho_M > \rho_\Lambda$. The conversion is very efficient. Details will be in Sec. 7.1.
- (iii) The coupled case is $\Gamma_M/H > 1$ and $\rho_M^H \approx \rho_M$, when ρ_M^H tightly couples with ρ_M in the Universe evolution of the Hubble time scale τ_H . Dark energy and matter exchange rate $\delta Q = \Gamma_M (\rho_M^H - \rho_M) \approx 0$ is very small. Dark energy is almost constant in time $\dot{\rho}_\Lambda \approx 0$. It is the case for the matter-dominated episode in reheating, see Sec. 7.2, and for stable massive pairs (cold dark matter) evolution, see Sec. 9.
- (iv) In case (iii), $\delta Q \approx 0$ has two possibilities: (a) $\delta Q \gtrsim 0$ and $\rho_M^H \gtrsim \rho_M$, dark energy slowly converts to matter $\dot{\rho}_\Lambda \lesssim 0$; (b) $\delta Q \lesssim 0$ and $\rho_M^H \lesssim \rho_M$, matter slowly converts to dark energy $\dot{\rho}_\Lambda \gtrsim 0$. The (b) is the case for epochs after reheating. Dark energy converts to matter and reduces to its minimal value in reheating, and matter and radiation become dominant over (much larger than) dark energy. However, dark energy weakly couples to matter and radiation, i.e., $\delta Q \approx 0$ and $\dot{\rho}_\Lambda \approx 0$. Its variation is much more slowly than matter/radiation decrease. Then it dominates over matter and radiation today. We present the preliminary discussions in Ref. [53].

The inclusion of decay terms $\Gamma_M^{\text{de}} \rho_M$ and transitions from one case to another are complex and need numerical studies.

5.2 Unstable massive pair decay and reheating equation

Coming from massive unstable pairs' decay, the radiation energy density ρ_R of relativistic particles $\bar{\ell}\ell$ (5.6) obeys the energy conservation law, see for example Ref. [49],

$$\begin{aligned} d(a^3 \rho_R) &= -p_R d(a^3) - d(a^3 \rho_M) \\ &= -\frac{\rho_R}{3} d(a^3) + (a^3 \rho_M) \Gamma_M^{\text{de}} dt, \end{aligned} \quad (5.9)$$

⁸In Ref. [41], we approximately neglect ρ_M and cosmic rate equation (5.5) to obtain an analytical solution.

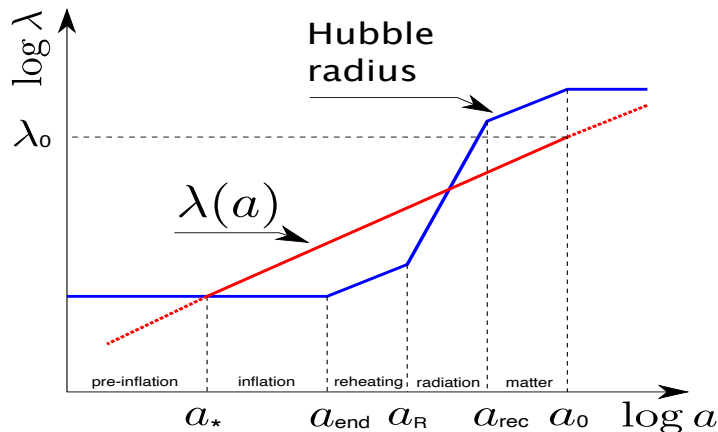


Figure 2. We make this figure by modifying Fig. 1 in Ref. [54]. Schematic evolution of the Hubble radius H^{-1} and the physical length scale $\lambda(a)$, where physically interested scale $\lambda_0 = \lambda(a_0)$ at the present time $a_0 = 1$ crossed the Hubble horizon H_* at the early time a_* , fixed by the CMB pivot scale $\lambda_0 = \lambda_* = k_*^{-1}$. The pre-inflation $a > a_*$, the inflation $a_* < a < a_{\text{end}}$, the reheating $a_{\text{end}} < a < a_R$, and the recombination at a_{rec} .

where $d(a^3 \rho_M) = -(a^3 \rho_M) \Gamma_M^{\text{de}} dt$ is the massive pair energy, that converts to radiation energy. It leads to the reheating equation

$$\dot{\rho}_R + 4H\rho_R = \Gamma_M^{\text{de}} \rho_M. \quad (5.10)$$

As a result, we have a close set of four ordinary differential equations to uniquely determine the time evolution of the Hubble rate H , dark-energy density ρ_Λ , massive particles' energy density ρ_M and relativistic particles' energy density ρ_R . They are generalised Friedman equations (2.2,2.3) for H and ρ_Λ , the cosmic rate equation (5.5) for ρ_M , and the reheating equation (5.10) for ρ_R . In addition, there are four algebraic relations: the massive pair plasma density ρ_M^H (4.1), the pair-production rate Γ_M (5.1), the Universe evolution ϵ -rate (5.2) and the pair-decay rate Γ_M^{de} (5.6). We will numerically solve these equations, provided initial conditions are known.

6 Initial conditions and basic equations for reheating

The inflation epoch ($H > \Gamma_M$) ends, and the reheating epoch ($H < \Gamma_M$) starts. The transitioning process must be very complex due to the back reactions of microscopic and macroscopic processes. We assume the transition to be instantaneous at the inflation end a_{end} and H_{end} when $H \lesssim \Gamma_M$. For the inflation epoch from a_* to a_{end} , see Figure 2, we obtain [41]

$$H_{\text{end}} = H_* e^{-\epsilon_* N_{\text{end}}}, \quad \epsilon_* = \chi(m_*/m_{\text{pl}})^2, \quad \Delta_3 \equiv (a_{\text{end}}/a_*) = e^{N_{\text{end}}} \quad (6.1)$$

where the inflation scale H_* and a_* correspond to the pivot scale $k_* = 0.05 \text{ (Mpc)}^{-1}$ crossed the horizon ($k_* = H_* a_*$) for CMB observations [55]. The observed spectral

index n_s and scalar amplitude A_s determine $H_* = 3.15 \times 10^{-5} (r/0.1)^{1/2} m_{\text{pl}}$ and the $\epsilon_* = (1 - n_s)/2 \approx 0.0175$ of the ϵ -rate (5.2) in inflation. The e -folding number N_{end} and the tensor-to-scalar ratio r are related by $H_{\text{end}} \lesssim \Gamma_M$

$$r \lesssim 7.97 \times 10^4 \chi (1 - n_s)^3 e^{(1 - n_s)N_{\text{end}}}, \quad (6.2)$$

and $\chi > 0$ implies $r > 0$. The observational constraint on the tensor-to-scalar ratio and spectra index (r, n_s) , see Fig. 2 of Ref. [41], gives $\chi \lesssim \mathcal{O}(10^{-3})$. The small H variation implies at the inflation end

$$H_{\text{end}}^2 = \frac{\rho_{\Lambda}^{\text{end}} + \rho_M^{\text{end}}}{3m_{\text{pl}}^2} \approx \frac{\rho_{\Lambda}^{\text{end}}}{3m_{\text{pl}}^2}; \quad \rho_{\Lambda}^{\text{end}} \gg \rho_M^{\text{end}}, \quad (6.3)$$

and $\rho_{\Lambda}^{\text{end}} \approx \rho_c^{\text{end}} \equiv 3m_{\text{pl}}^2 H_{\text{end}}^2$. We approximately adopt the value

$$\Omega_M^{\text{end}} = \rho_M^{\text{end}} / \rho_c^{\text{end}} \approx 4.7 \times 10^{-3}, \quad (6.4)$$

for which $(\Gamma_M/H)_{\text{end}} \approx 1$. These are the reheating epoch initial conditions.

Using the characteristic scale H_{end} and density ρ_c^{end} , we normalize $h \equiv H/H_{\text{end}}$,

$$\Omega_{\Lambda, M, R} \equiv \frac{\rho_{\Lambda, M, R}}{\rho_c^{\text{end}}}, \quad \Omega_M^H \equiv \frac{\rho_M^H}{\rho_c^{\text{end}}} = \frac{2}{3} \chi (\hat{m}/m_{\text{pl}})^2 h^2. \quad (6.5)$$

Here we introduce the mass parameter \hat{m} or $\chi(\hat{m}/m_{\text{pl}})^2$ as a typical scale parameter for reheating and will fix its value by observations. Thus, we recast the Friedman equations (2.2) and (2.3), the cosmic rate equation (5.5) and reheating equation (5.10) as,

$$h^2 = \Omega_{\Lambda} + \Omega_M + \Omega_R, \quad (6.6)$$

$$\frac{dh^2}{dx} \approx -3\Omega_M - 4\Omega_R, \quad (6.7)$$

$$\frac{d\Omega_M}{dx} + 3\Omega_M = \frac{\Gamma_M}{H} (\Omega_M^H - \Omega_M) - \frac{\Gamma_M^{\text{de}}}{H} \Omega_M, \quad (6.8)$$

$$\frac{d\Omega_R}{dx} + 4\Omega_R = \frac{\Gamma_M^{\text{de}}}{H} \Omega_M. \quad (6.9)$$

The ratios are

$$\frac{\Gamma_M}{H} = \left(\frac{\chi}{4\pi} \right) \left(\frac{\hat{m}}{H_{\text{end}}} \right) \frac{\epsilon}{h}; \quad \frac{\Gamma_M^{\text{de}}}{H} = g_Y^2 \left(\frac{\hat{m}}{H_{\text{end}}} \right) \frac{1}{h}, \quad (6.10)$$

and the ϵ -rate (5.2) becomes

$$\epsilon \equiv -\frac{1}{H} \frac{dH}{dx} = \frac{3\Omega_M + (4/3)\Omega_R}{2\Omega_{\Lambda} + \Omega_M + \Omega_R}. \quad (6.11)$$

Instead of the cosmic time t , here we adopt the cosmic e -folding variable $x = \ln(a/a_{\text{end}})$ and $d(\dots)/dx = d(\dots)/(Hdt)$ for the sake of simplicity and significance in physics. In

the next sections, we will numerically integrate these basic equations (6.6-6.11) for the reheating epoch by using the inflation end (6.4) as the initial condition.

We have to emphasize that the differential equations (6.6-6.9) represent a macroscopic back-and-forth reaction system characterized by the scales τ_H , τ_M and τ_R . It describes the processes: inflation, reheating and standard cosmology. It differs from the differential equations (2.4-2.5) and those in Sec. 3 for a microscopic back-and-forth reaction system of fast-oscillating components characterized by the scale $\mathcal{O}(1/M)$. The fast components' contributions are effectively represented by the massive pair plasma state ρ_M^H (4.1) that enters the cosmic rate equation (6.8).

7 Different episodes in reheating epoch

In the reheating epoch, generally speaking, the horizon h and the dark energy Ω_Λ decreases, as the matter content Ω_M or Ω_R increases, meanwhile the ratio Γ_M/H (6.10) and the ϵ -rate (6.11) increase. To gain insight into the physics first, we use the ϵ -rate values (6.11) to characterize the different episodes in the reheating epoch. In each episode, the ϵ rate slowly varies in time, we approximately have the time scale of the spacetime expansion $H^{-1} \approx \epsilon t$. In the transition from one episode to another, the ϵ -rate significantly changes its value. Using the characteristic ϵ values $\epsilon \ll 1$, $\epsilon \approx 3/2$, $\epsilon \approx 2$, we identify the following three different episodes \mathcal{P} -episode, \mathcal{M} -episode and \mathcal{R} -episode in the reheating epoch.

7.1 Preheating \mathcal{P} -episode: dark energy ρ_Λ converting into matter ρ_M

The short preheating \mathcal{P} -episode is the transition from the inflation end to the reheating start. In this episode, the pair production rate Γ_M (5.1) is larger than the Hubble rate H , that is still much larger than the pair decay rate Γ_M^{de} (5.6),

$$\Gamma_M > H \gg \Gamma_M^{\text{de}}, \quad \rho_\Lambda > \rho_M^H > \rho_M \gg \rho_R. \quad (7.1)$$

The radiation energy density is completely negligible $\rho_R \approx 0$. We neglect massive pairs decay to light particles $\Gamma_M^{\text{de}} \approx 0$ (5.6). The reheating equation (6.9) is then not relevant, and the basic equations (6.6), (6.7) and (6.8) reduce to

$$h^2 = \Omega_\Lambda + \Omega_M, \quad (7.2)$$

$$dh^2/dx = -3\Omega_M, \quad (7.3)$$

$$d\Omega_M/dx + 3\Omega_M = (\Gamma_M/H) (\Omega_M^H - \Omega_M), \quad (7.4)$$

where the ratio $\Gamma_M/H > 1$ (6.10) increases as the ϵ -rate (6.11)

$$\epsilon \approx \frac{3}{2} \frac{\rho_M}{\rho_\Lambda + \rho_M} = \frac{3}{2} \frac{\Omega_M}{\Omega_\Lambda + \Omega_M}. \quad (7.5)$$

In the \mathcal{P} -episode, these equations uniquely determine the evolution of the Hubble rate H , pairs' energy densities ρ_M and dark-energy density ρ_Λ .

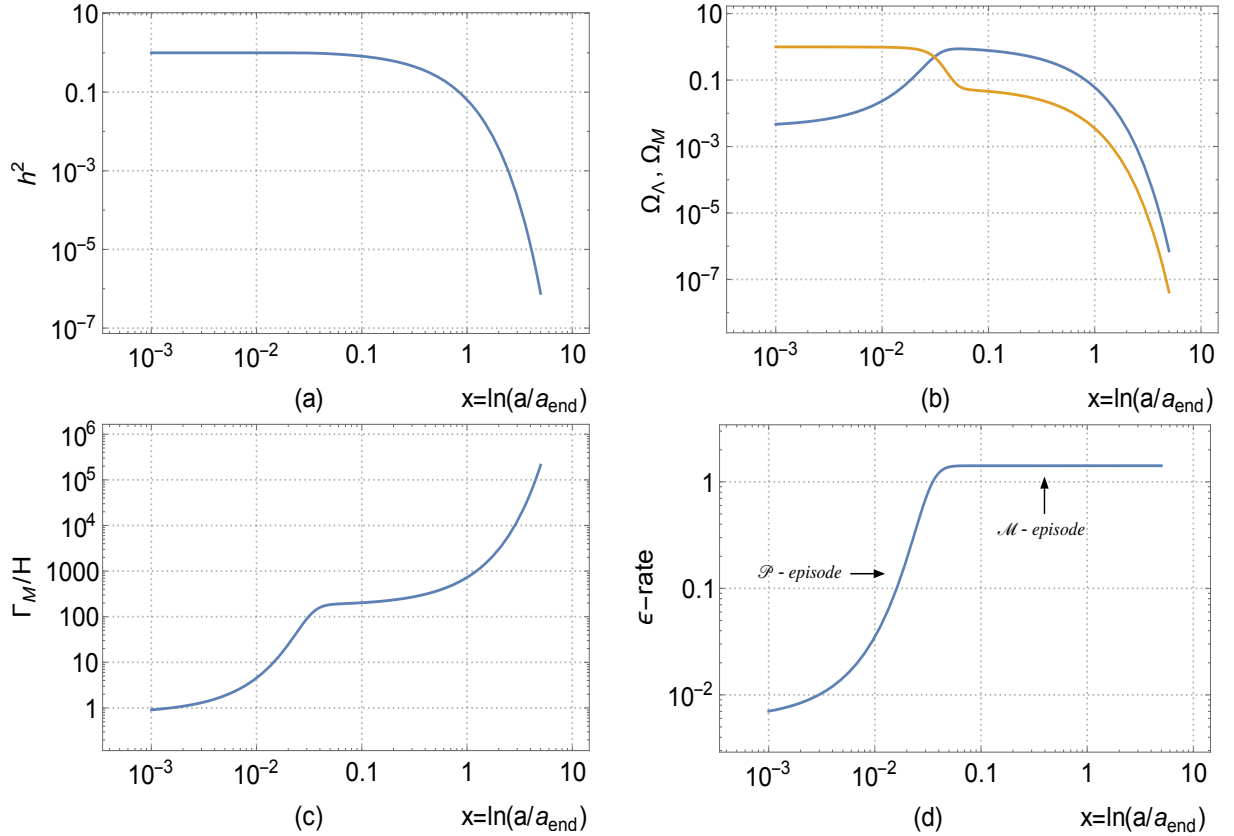


Figure 3. (Color Online). In a few e -folding number $x = \ln(a/a_{\text{end}})$, (a) the Hubble rate drops rapidly; (b) the massive pair energy density exceeds the dark-energy density; (c) the ratio $\Gamma_M/H > 1$ increases rapidly; (d) the ϵ -rate of H variation increases in the transition from $\epsilon \ll 1$ (inflation epoch) to the asymptotic value $\epsilon \sim \mathcal{O}(1)$ (\mathcal{M} -episode, see Sec. 7.2). We plot these solutions with the initial condition (6.4) and parameter $(\hat{m}/m_{\text{pl}}) = 27.7$.

7.1.1 High efficiency of dark energy converting into matter

Using the values H_{end} (6.1) and Ω_M^{end} (6.4) at the inflation end as the initial conditions for the \mathcal{P} -episode, we numerically integrate Eqs. (6.6), (6.7) and (6.8), by selecting values of the mass parameter \hat{m}/m_{pl} . In Figs. 3 and 4, the numerical solutions are plotted in terms of the e -folding variable $x = \ln(a/a_{\text{end}})$. These solutions show an important result that the dark-energy density ρ_Λ is significantly converted to the matter-energy density ρ_M , as the pair-production rate Γ_M increases and becomes much larger than the Hubble rate H . In more detail, we list that in the \mathcal{P} -episode the physical quantities vary in time as follows,

- (i) the Hubble rate h decreases rapidly in a few e -folding number, as ρ_M becomes dominate over ρ_Λ , see Fig. 3 (a);
- (ii) the ρ_M increases at the expense of the ρ_Λ , eventually ρ_M exceeds and dominates ρ_Λ , see Fig. 3 (b);

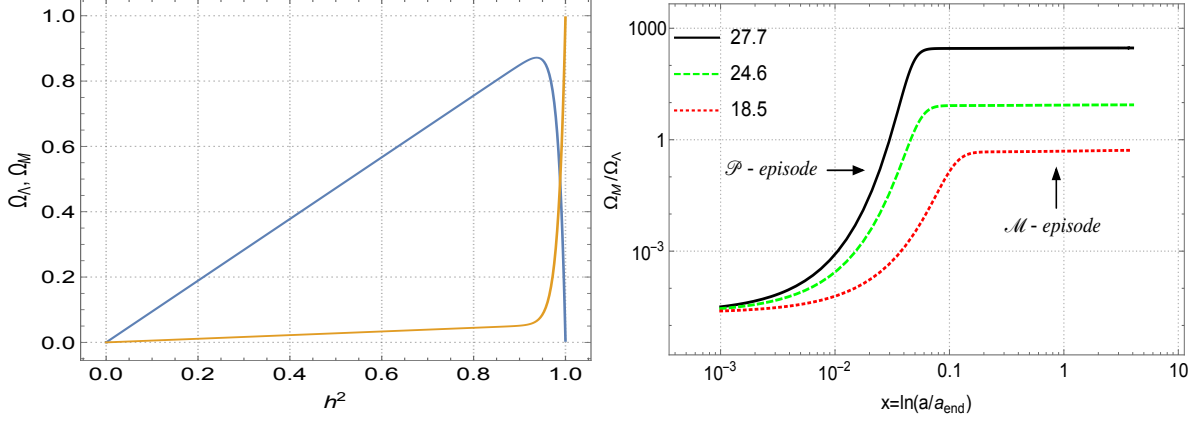


Figure 4. (Color Online). Left: The energy densities Ω_Λ (orange) and Ω_M (blue) are plotted as functions of the horizon h^2 , corresponding to Figs. 3 (a) and (b). Right: The ratio $\Omega_M/\Omega_\Lambda = \rho_M/\rho_\Lambda$ varies in the transition from $\rho_M/\rho_\Lambda \ll 1$ (inflation epoch) to $\rho_M/\rho_\Lambda \gg 1$, approaching to a constant (\mathcal{M} -episode). We plot the ratio ρ_M/ρ_Λ for selected values $\hat{m}/m_{\text{pl}} = 27.7, 24.6, 18.5$, corresponding to the solid black line, green dashed line, red dotted line. The initial conditions are H_{end} (6.1) and Ω_M^{end} (6.4).

- (iii) the ratio Γ_M/H (7.1) increases and becomes much larger than unity ($\Gamma_M/H \gg 1$), see Fig. 3 (c);
- (iv) the H varying rate ϵ (7.5) increases from $\epsilon \ll 1$ to $\epsilon \sim \mathcal{O}(1)$, indicating the transition from the inflation end to the preheating \mathcal{P} -episode, and it then approaches to an asymptotic value, see Fig. 3 (d).

In Figure 4 (left), we plot the energy densities Ω_Λ and Ω_M as functions of the horizon h^2 , corresponding to Figures (a) and (b) in Fig. 3. It shows two branches of asymptotic solutions Ω_Λ (orange) respectively,

$$\Omega_\Lambda \simeq \alpha_\Lambda^1 h^2 \quad (h^2 < 0.95); \quad \Omega_\Lambda \simeq \alpha_\Lambda^2 h^2 \quad (h^2 > 0.95); \quad \alpha_\Lambda^2 \gg \alpha_\Lambda^1, \quad (7.6)$$

$\Omega_M + \Omega_\Lambda = h^2$ and the turning point is about $h^2 \approx 0.98$, at which Ω_M exceeds Ω_Λ and the rapid $\rho_\Lambda \Rightarrow \rho_M$ converting process takes place. The characteristic behaviour $\Omega_\Lambda \propto h^2$ (7.6) is the same as that in the pre-inflation and inflation epochs. Correspondingly, two branches of asymptotic solutions for the matter Ω_M (blue) are

$$\Omega_M \simeq \alpha_M^1 h^2 \quad (h^2 < 0.95); \quad \Omega_M \simeq \Omega_M^{\text{max}} - \alpha_M^2 (h^2 - 0.95) \quad (h^2 > 0.95), \quad (7.7)$$

and $\alpha_M^2 \gg \alpha_M^1$, where $\Omega_M^{\text{max}} \approx 0.85$ when $h^2 \approx 0.95$. The coefficients $\alpha_\Lambda^{1,2}$ and $\alpha_M^{1,2}$ in Eqs. (7.6) and (7.7) can be numerically obtained. As $h^2 \rightarrow 0$ and (a/a_{end}) increases, $\Omega_M \rightarrow 0$, $\Omega_\Lambda \rightarrow 0$ and $\Omega_M \gg \Omega_\Lambda$ ($\alpha_M^1 \gg \alpha_\Lambda^1$).

Figure 4 (right) shows that in the preheating \mathcal{P} -episode, the dark energy density ρ_Λ converts to the matter-energy ρ_M . The ratio ρ_M/ρ_Λ rapidly increases in a few e -folding numbers from $\rho_M/\rho_\Lambda \ll 1$ at the inflation end to a value $\rho_M/\rho_\Lambda \gtrsim \mathcal{O}(1)$. Then ρ_M becomes dominant. The Hubble rate H rapidly decreases and becomes much

smaller than the pair-production rate Γ_M . We define the \mathcal{P} -episode end at $1.11a_{\text{end}}$ by $\rho_\Lambda \approx \rho_M$ from Figs. 3 and 4 (right). It shows that the preheating \mathcal{P} -episode is a very brief transition episode.

We ought to discuss the condition for high efficiency of dark energy converting into massive pairs' energy in this preheating \mathcal{P} -episode. Figure 3 (b) shows ρ_Λ decreases and ρ_M increases rapidly, the efficiency of dark energy converting matter-energy is large. The reasons are the following. (i) The ratio $\Gamma_M/H \gg 1$ increases rapidly as H decreases rapidly, see Fig. 3 (c) and (a), respectively. (ii) The ϵ rate (5.2) rapidly increases to the order of unity, see Fig. 3 (d). (iii) The mass parameter \hat{m} (5.1) is large, see Fig. 4 (right), which implies heavy mass M and large number $\mathcal{N}_{\text{pair}}$ of pairs produced in the massive pair plasma state (4.1). If the mass parameter \hat{m} is small, the dark energy and matter conversion efficiency is small, see the ratio Ω_M/Ω_Λ in Fig. 4 (right). *A priori*, we do not have theoretical arguments about how much \hat{m} value is. Instead, we select \hat{m} values *a posteriori* in comparison with observations, and the Universe does not stay cold state of $\rho_\Lambda > \rho_M$. The necessary condition is the existence of a threshold \hat{m}_{thresh} for which $\rho_M > \rho_\Lambda$ of efficient conversion in reheating.

7.1.2 Threshold of massive pair mass and number for $\rho_M > \rho_\Lambda$

Figure 4 (right) shows an important result. These solutions depend on the pair mass parameter \hat{m} (4.1) introduced for the reheating epoch. There exists a theoretical threshold on the mass parameter $\hat{m}_{\text{thresh}} \approx 20m_{\text{pl}}$.

- (a) For large mass parameters $\hat{m}/m_{\text{pl}} > 20$, the pair energy density ρ_M exceeds the dark-energy density ρ_Λ and the asymptotic value $\rho_M/\rho_\Lambda > 1$,

$$\hat{m} > \hat{m}_{\text{thresh}} \approx 20m_{\text{pl}}, \quad \rho_M/\rho_\Lambda > 1. \quad (7.8)$$

The reason is that the number $\mathcal{N}_{\text{pair}}$ (or effective degeneracy g_d) of massive pairs produced in the reheating epoch has to be large enough so that $\Gamma_M \gg H$ and the conversion from ρ_Λ to ρ_M is efficient. It corresponds to the physical situation that the most radiation and matter of the Universe is generated in the reheating epoch.

- (b) For small mass parameters $\hat{m}/m_{\text{pl}} < 20$, the massive pairs' energy density ρ_M never exceeds the dark-energy density ρ_Λ , namely $\rho_M/\rho_\Lambda < 1$. The conversion from ρ_Λ to ρ_M is inefficient. This case corresponds to the unrealistic situation that the Universe inflation would never have completely ended, i.e., the cosmological term ρ_Λ always dominates H^2 .

Observe that the mass parameter \hat{m} of the reheating epoch is larger than the mass parameter m_* of the inflation epoch. From the viewpoint of pair production, the pair mass scale in reheating should be smaller than that in inflation since the reheating horizon H is smaller than the inflation one. Therefore, it implies that the effective numbers $\mathcal{N}_{\text{pair}}$ of massive pairs produced in reheating, $\Gamma_M/H > 1$ is much larger than that of massive pairs produced in inflation $\Gamma_M/H < 1$. These massive pairs contain both stable and unstable pairs.

Equation (7.5) shows that the asymptotic value of the Horizon variation ϵ -rate (5.2) relates to the ratio ρ_M/ρ_Λ asymptotic value, see Figs. 3 (d) and 4 (right). For large mass parameter $\hat{m}/m_{\text{pl}} \gtrsim 27.7$, the ratio $\rho_M/\rho_\Lambda \gg 1$ ⁹, the ϵ -rate (7.5) approaches to the asymptotic value $\epsilon \approx \epsilon_M = 3/2$. It shows the episode of massive pairs domination: *M-episode*.

7.1.3 Minimal comoving radius $(Ha)^{-1}$ location

Before discussing the *M-episode*, we would like to mention the turning point at which the Universe acceleration vanishes $\ddot{a} = 0$,

$$2\rho_\Lambda = (1 + 3\omega_M)\rho_M - (1 + 3\omega_R)\rho_R, \quad (7.9)$$

which is obtained from the 1–1 component of the Einstein equation

$$2\frac{dH}{dt} + 2H^2 = \frac{2\ddot{a}}{a} = \left[2\rho_\Lambda - (1 + 3\omega_M)\rho_M - (1 + 3\omega_R)\rho_R \right]. \quad (7.10)$$

At this turning point, the Universe stops acceleration $\ddot{a} > 0$ and starts deceleration $\ddot{a} < 0$. The turning point occurs at $\rho_\Lambda = \rho_M/2$ for $\omega_M \approx 0$ and $\rho_R \approx 0$. It tells us the balance point of the competition between ρ_Λ and ρ_M in the *P-episode*.

On the other hand, the minimal value of the comoving radius $(aH)^{-1}$ locates at

$$d(aH)^{-1}/dt = 0 \quad \Rightarrow \quad \dot{H} + H^2 = 0. \quad (7.11)$$

From Friedman equations (2.1), we obtain

$$\rho_\Lambda = \rho_M/2 + \rho_R \approx \rho_M/2, \quad \epsilon = \epsilon_\Lambda^{\text{min}} = 1, \quad (7.12)$$

coinciding with the turning point (7.9). Namely at the minimal comoving radius $(aH)^{-1}$, the Universe stops acceleration $\ddot{a} > 0$ and begins deceleration $\ddot{a} < 0$, starting the reheating epoch and standard cosmology. This is indeed the case for large mass parameter $(\hat{m}/m_{\text{pl}}) > 20$ and the ratio ρ_M/ρ_Λ becomes larger than 2. The numerical results (Fig. 3) show that this turning/minimal point $\epsilon_{\text{min}} = 1$ locates at $x_{\text{min}} \approx 1.7 \times 10^{-2}$ and $a_{\text{min}} \approx a_{\text{end}} \times \exp(1.7 \times 10^{-2}) = 1.02 a_{\text{end}}$.

While the turning/minimal point $\epsilon_{\text{min}} = 1$ is never reached, for the cases of the small mass parameter $(\hat{m}/m_{\text{pl}}) < 20$ and the ratio ρ_M/ρ_Λ is always smaller than 2, see Fig. 4 (right). The reason is that dark energy converting to matter is inefficient, the massive pairs energy is not large enough to balance the dark energy and slow down the Universe's acceleration. The Universe keeps acceleration $\ddot{a} > 0$ and does not run into the reheating epoch. Therefore, the mass parameter range below the threshold \hat{m}_{thresh} (7.8) $(\hat{m}/m_{\text{pl}}) < 20$ should be excluded.

⁹This condition also admits the possibility of a small negative dark energy density $\rho_\Lambda < 0$ and $|\rho_\Lambda| \ll \rho_M$. Namely, Figure 3 (b) admits solution $\rho_M \gg |\rho_\Lambda|$ and ρ_Λ drops slightly below zero.

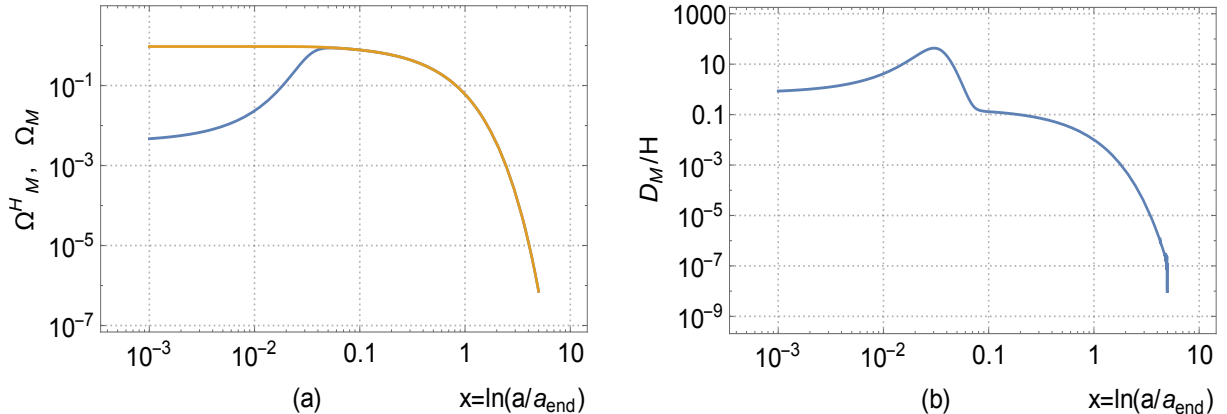


Figure 5. (Color Online). In a few e -folding number $x = \ln(a/a_{\text{end}})$, (a) the energy density ρ_M^H (6.5) (orange) and the solution ρ_M (blue) to the cosmic rate equation (7.4), showing ρ_M approaches ρ_M^H ; (b) the detailed balance term D_M (7.15) vanishes. We plot these solutions with the initial condition (6.4) and parameter $(\hat{m}/m_{\text{pl}}) = 27.7$.

7.2 Massive pairs domination: \mathcal{M} -episode

After the \mathcal{P} -episode transition, it is the \mathcal{M} -episode of massive pair domination characterised by

$$\rho_M \gg \rho_\Lambda \gg \rho_R, \quad \Gamma_M > H > \Gamma_M^{\text{de}}. \quad (7.13)$$

The radiation energy density ρ_R is negligible in the basic equations (6.6-6.11). The H variation ϵ -rate $\epsilon_M \approx 3/2$ in Fig. 3 (d) for $\rho_M/\rho_\Lambda \gg 1$ in Fig. 4 (right). In this episode, the Hubble rate H and scale factor $a(t)$ vary as

$$H^{-1} \approx \epsilon_M t, \quad a(t) \sim t^{1/\epsilon_M}, \quad (7.14)$$

$h^2 \approx \Omega_M$ and the pair energy density $\Omega_M \propto (a/a_{\text{end}})^{-2\epsilon_M}$.

Moreover, the back-and-forth processes (5.3) are important, as described by the cosmic rate equation (7.4) with the detailed balance term D_M ,

$$D_M \equiv \Gamma_M (\Omega_M^H - \Omega_M), \quad (7.15)$$

and we define its characteristic time scale τ_D

$$\tau_D^{-1} \equiv \frac{D_M}{\Omega_M} = \frac{\Gamma_M}{\Omega_M} (\Omega_M^H - \Omega_M). \quad (7.16)$$

Note that τ_D differs from $\tau_M = \Gamma_M^{-1}$ (5.1). The microscopic time scale τ_M is much smaller than the macroscopic expansion time scale $\tau_H = H^{-1}$, $\tau_M \ll \tau_H$. Therefore, the back-and-forth (5.3) can build an energy equipartition $\rho_M \approx \rho_M^H$, and the detailed balance term (7.15) vanish in its time-averaged

$$\langle \rho_M - \rho_M^H \rangle = 0, \quad (7.17)$$

over the macroscopic time $\tau_H \gg \tau_M$. The cosmic rate equation becomes approximately

$$\frac{d\rho_M}{dt} + 3H\rho_M \approx 0, \quad (7.18)$$

whose solution is $\rho_M \propto a^{-3}$. It is consistent with the matter-dominated solution to Eq. (2.3), yielding $H^2 \sim \rho_M \propto a^{-3}$. It is also self-consistent with the pair plasma density (4.1) $\rho_M^H = 2\chi\hat{m}^2 H^2 \propto a^{-3}$.

In order to verify these discussions and $\rho_M \approx \rho_M^H$, we check the solution (7.17) or (7.18) analytically and numerically. The $\rho_M^H = 2\chi\hat{m}^2 H^2$ averaged over the time τ_H consistently obeys the same equation (7.18) for ρ_M ,

$$\langle \dot{\rho}_M^H \rangle = \langle 4\chi\hat{m}^2 H\dot{H} \rangle = -\langle 2H\rho_M^H \epsilon \rangle \approx -3H\rho_M^H, \quad (7.19)$$

where $\langle \epsilon \rangle \approx \epsilon_M = 3/2$. Numerical results quantitatively show the same conclusion $\rho_M \approx \rho_M^H$, see Fig. 5 (a), and the detailed balance term (7.15) vanishes, see Fig. 5 (b). Thus we conclude that in the \mathcal{M} -episode, due to $\Gamma_M \gg H$ and $\tau_M \ll \tau_H$, the massive pairs plasma state ρ_M^H tightly couples with the mass density ρ_M in the H evolution.

7.3 Relativistic particles domination: \mathcal{R} -episode of genuine reheating

At the end of the \mathcal{M} -episode, the massive pairs' decay term $\Gamma_M^{\text{de}}\rho_M$ in equations (6.8,6.9) starts to dominate, when the time $t \gtrsim \tau_R$. The τ_R (5.6) is the characteristic time scale of massive pairs decay to relativistic particles. It represents the reheating period of producing tremendous amounts of entropy. The reheating epoch starts its genuine reheating episode, i.e., \mathcal{R} -episode.

7.3.1 Massive and unstable pairs decay to relativistic particles

To study the \mathcal{R} -episode, we numerically solve the closed set of the basic equations (6.6-6.9) with the radiation energy density Ω_R and the decay term,

$$R_M = \Gamma_M^{\text{de}}\Omega_M, \quad \tau_R^{-1} \equiv (R_M/\Omega_M) = \Gamma_M^{\text{de}}, \quad (7.20)$$

and we define the characteristic time scale of the decay term R_M , which is the same as τ_R (5.6). The initial condition of the radiation energy density is $\Omega_R^{\text{end}} = 0$ at the inflation end a_{end} , in addition to the initial conditions (6.1) and (6.4). We report the numerical results in Figures 6. It shows that in the H^2 (6.6), the radiation energy density Ω_R increases and becomes dominant, compared with Ω_M and Ω_Λ .

We explain this phenomenon by comparing the decay term R_M (7.20) with the detailed balance term D_M (7.15) in the cosmic rate equation (6.8). Two different dynamics D_M and R_M compete with each other in the process. The ρ_R is negligible when $D_M > R_M$, while the ρ_R is dominant when $R_M > D_M$, and the transition from one to another occurs approximately at $R_M \gtrsim D_M$, where $\rho_R \lesssim h^2$, as shown in Figs. 7 (a) and (b). More precisely, it is the comparison between the characteristic time scale τ_D (7.16) of the back-and-forth process (5.3) and the characteristic time scale τ_R (7.20) of the pair decay process (5.6). When $\tau_D < \tau_R$, the faster back-and-forth process (5.3) dominates, whereas $\tau_R < \tau_D$, the faster decay process (7.21) dominates.

In Figs. 7 (c) and (d), two-time scales τ_D and τ_R are plotted as dimensionless quantities τ_D/τ_H and τ_R/τ_H to show two episodes:

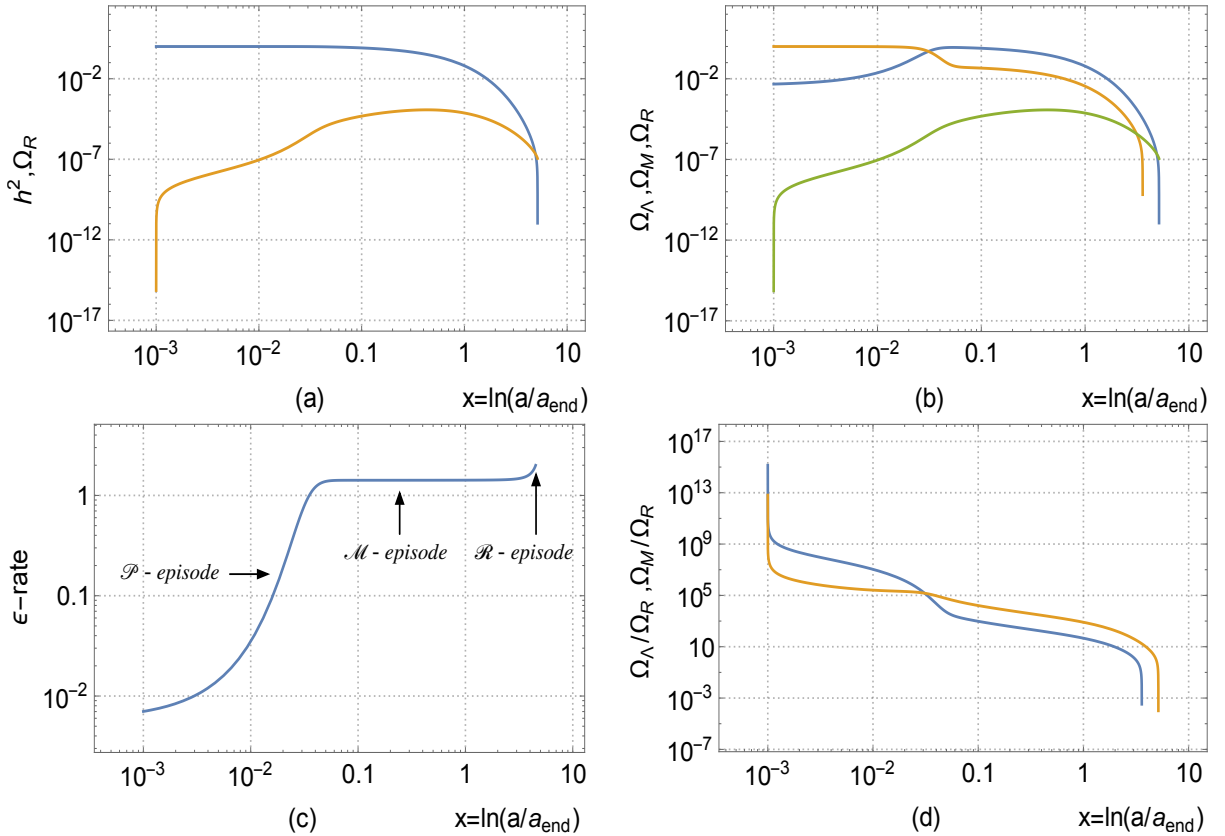


Figure 6. (Color Online). In a few e -folding number $x = \ln(a/a_{\text{end}})$, (a) the blue line h^2 and orange line Ω_R , the Hubble rate drops more rapidly than the neglecting Ω_R case, see Fig. 3 (a); (b) Ω_R, Ω_M and Ω_Λ are lines green, blue, and orange; (c) the H variation ϵ -rate increases in the transition from $\epsilon \ll 1$ (\mathcal{P} -episode) to the asymptotic value $\epsilon \sim \mathcal{O}(1)$ (\mathcal{M} -episode) and approaches to $\epsilon = 2$ (\mathcal{R} -episode); (d) the ratios of Ω_M/Ω_R (orange) and Ω_Λ/Ω_R (blue), recalling $h^2 = \Omega_\Lambda + \Omega_M + \Omega_R$. We plot these solutions with the initial conditions (6.4) and $\Omega_R^{\text{end}} = 0.0$, the parameter $(\hat{m}/m_{\text{pl}}) = 27.7$ and $g_Y^2 = 10^{-9}$.

- (i) the \mathcal{M} -episode, $\tau_D < \tau_R$ ($D_M > R_M$), indicating the back-and-forth process (5.3) dominates over the decay process (5.6);
- (ii) the \mathcal{R} -episode, $\tau_D > \tau_R$ ($D_M < R_M$), indicating the decay process (5.6) dominates over the back-and-forth process (5.3).

The separatrix of two episodes locates at $\tau_D \approx \tau_R$ ($D_M \approx R_M$), i.e., the crossing point of blue and orange lines in Figs. 7. It roughly gives the a_R value at which the genuine reheating occurs.

The a_R value decreases as the Yukawa coupling g_Y increases, shown by the left column (a,c) and the right column (b,d) of Figs. 7. Around this point a_R , Figures 6 (b) and (d) show $\Omega_R \gg \Omega_M \gg \Omega_\Lambda$, and Fig. 6 (c) shows $\epsilon \rightarrow 2$, indicating the radiation domination. At $a = a_R$, the numerical calculations of the equations (6.6-6.9) run into

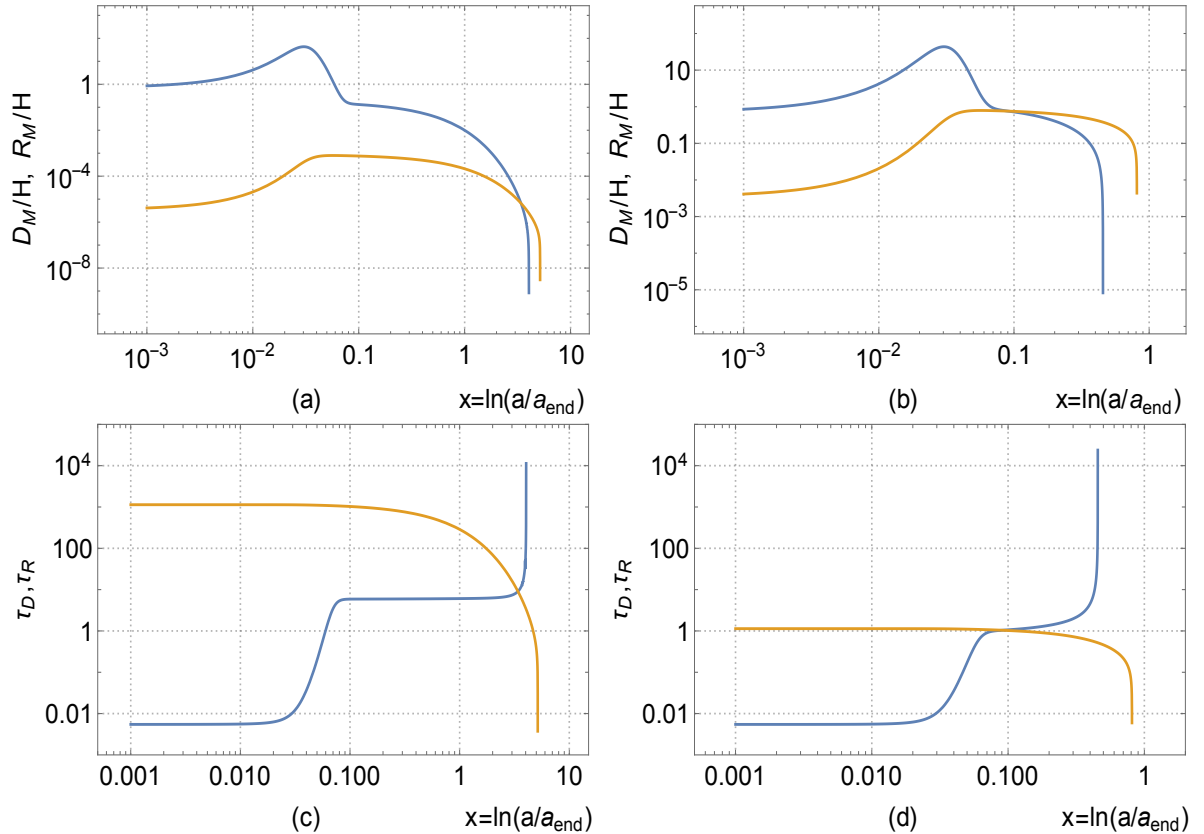


Figure 7. (Color Online). Plotted as a function of the e -folding variable $x = \ln(a/a_{\text{end}})$ for the same initial conditions and parameters in Figures 6, the detailed balance term D_M/H (7.15) (blue) and the decay term R_M/H (7.20) (orange); two time scales τ_D/τ_H (blue) and τ_R/τ_H (orange). Left column (a) and (c) for $g_Y^2 = 10^{-9}$ and $a_R \gtrsim 20.1a_{\text{end}}$; Right column (b) and (d) for $g_Y^2 = 10^{-6}$ and $a_R \gtrsim 1.8a_{\text{end}}$.

the stiffness system of step size being effective zero. However, the analytical solution to these basic equations is studied in the next section.

7.3.2 Energy densities of massive pairs and relativistic particles

The \mathcal{R} -episode is characterised by

$$\rho_R \gg \rho_M \gg \rho_\Lambda, \quad \epsilon \rightarrow \epsilon_R \approx 2, \quad (7.21)$$

and $\Gamma_M^{\text{de}}/H > 1$, as shown in Figs. 6. As a result, Equations (6.6) and (6.7) or Eq. (6.11) give

$$H^{-1} \approx \epsilon_R t, \quad a(t)/a_R \approx (t/\tau_R)^{1/\epsilon_R}. \quad (7.22)$$

Following the line presented in Ref. [49], we discuss how the massive pairs transfer their mass energy to relativistic particles, and calculate the radiation energy density ρ_R , entropy S and temperature T of relativistic particles.

Since unstable massive pairs predominately decay to relativistic particles, the detailed balance term D_M (7.15) is negligible, and the cosmic rate equation (6.8) reduces to,

$$\frac{d(a^3\rho_M)}{dt} = a^3\frac{d\rho_M}{dt} + 3Ha^3\rho_M \approx -\tau_R^{-1}a^3\rho_M, \quad (7.23)$$

$$\Rightarrow \rho_M \approx \rho_M(a_R) \left(\frac{a}{a_R}\right)^{-3} \exp -t/\tau_R. \quad (7.24)$$

The reheating equation (6.9) becomes

$$\frac{d(a^4\rho_R)}{dt} = a^3\frac{\rho_M(a_R)}{\tau_R} \left(\frac{a}{a_R}\right)^{-3} \exp -t/\tau_R. \quad (7.25)$$

In theory, it requires the the time integration from the initial time $t_i(a_i) \ll \tau_R$ when $\rho_R(a_i) = 0$ to the final time $t_f \gg \tau_R$ to obtain the radiation energy density ρ_R ,

$$\rho_R = \left(\frac{a_R}{a}\right)^4 \frac{\rho_M(a_R)}{\tau_R} \int_{t_i}^{t_f} \left(\frac{t}{\tau_R}\right)^{1/\epsilon_R} e^{-t/\tau_R} dt \approx 0.89 \left(\frac{a_R}{a}\right)^4 \rho_M(a_R). \quad (7.26)$$

Through their gauge and other induced interactions, these relativistic particles $\bar{\ell}\ell$ including sterile particles and other particles beyond the SM interact with each other. They are quickly thermalised at a very high temperature T , due to their high number and energy densities. The local thermalisation time scale is much shorter than the expansion time scale $\tau_H = H^{-1}$, and thus the local thermal equilibrium is built.

7.3.3 Reheating temperature and entropy

We follow the approach [49] to calculate the reheating temperature and entropy. The second law of thermodynamics applied to a comoving volume element yields

$$dS = \frac{dQ}{T} = -\frac{d(a^3\rho_M)}{T} \approx \frac{a^3\rho_M}{T}\tau_R^{-1}dt, \quad (7.27)$$

where dQ is the pair mass energy and dS is the entropy of relativistic particles produced from massive pairs decay. Therefore, in a comoving volume, the entropy and energy densities of relativistic particles at the thermal state of temperature T are given by,

$$\rho_R = \frac{\pi^2}{30}g_*T^4, \quad S = \frac{2\pi^2}{45}g_*a^3T^3, \quad \rho_R = \frac{3}{4} \left(\frac{45}{2\pi^2g_*}\right)^{1/3} S^{4/3}a^{-4}. \quad (7.28)$$

The appropriately time-averaged degeneracy g_* over the decay period τ_R counts for the total number of effectively massless degrees of freedom, those species share a common temperature T . Using the entropy (7.28), one writes Eq. (7.27) as,

$$S^{1/3}\dot{S} = \left(\frac{2\pi^2g_*}{45}\right)^{1/3} a^4\rho_M\tau_R^{-1}. \quad (7.29)$$

Integrating this equation over the decay period τ_R from the initial scale factor a_i to the reheating scaling factor $a_R > a_i$ leads to an approximate solution

$$\begin{aligned} S_R^{4/3} &= 1.09 \left(\frac{4}{3} \rho_M(a_i) a_R^4 \right) \left(\frac{16\pi^3 g_* \rho_M(a_i)}{135 M_{\text{pl}}^2} \right)^{1/3} \tau_R^{2/3}, \\ \Rightarrow S_R &\approx 1.32 (16\pi^3 g_*/135)^{1/4} a_R^3 \rho_M(a_i) (\tau_R/M_{\text{pl}})^{1/2}. \end{aligned} \quad (7.30)$$

Here one adopts Eq. (7.24) and $S_i(a_i) \approx 0$, namely, the initial massive pairs' entropy is approximately zero. In principle, it requires integrating from the initial time $t_i(a_i) \ll \tau_R$ to the final time $t_f(a_R) \gg \tau_R$, when the entropy significantly increases. In practice, $a_i \lesssim a_R$ and $t_f \gtrsim \tau_R$ are approximately adopted in Eq. (7.30), since the all-important entropy S_R mainly produces in the reheating period $\tau_R(a_R)$.

At the scale factor a_R , the reheating scale H_{RH} can be obtained by τ_R from the Friedmann equation (6.6) or the reheating temperature $T_{\text{RH}} \equiv T(t = \tau_R)$ from the thermalization (7.28) [49]:

$$H_{\text{RH}}^2 \equiv H^2(t = \tau_R) \approx \frac{1}{4} \tau_R^{-2}, \quad (7.31)$$

$$H_{\text{RH}}^2 \approx \frac{8\pi}{3M_{\text{pl}}^2} \rho_R \approx \frac{8\pi}{3M_{\text{pl}}^2} \left(\frac{\pi^2 g_* T_{\text{RH}}^4}{30} \right). \quad (7.32)$$

It leads to the reheating temperature

$$T_{\text{RH}} \approx 0.55 g_*^{-1/4} (M_{\text{pl}}/\tau_R)^{1/2} = 0.55 (g_Y^2/g_*^{1/2})^{1/2} (\hat{m}/M_{\text{pl}})^{1/2} M_{\text{pl}}, \quad (7.33)$$

and the all-important entropy per comoving volume,

$$S_R \approx 1.32 \left(\frac{16\pi^3}{135} \right)^{1/4} (g_*^{1/2}/g_Y^2)^{1/2} (\hat{m}/M_{\text{pl}})^{1/2} a_R^3 \rho_M(a_i) / \hat{m}. \quad (7.34)$$

Equations (7.31) and (7.32) physically mean that at the the genuine reheating (i) $H_{\text{RH}} \approx \Gamma_M^{\text{de}}/2 = g_Y^2 \hat{m}/2$ the Hubble rate is in the same order as the pair decay rate; (ii) $H_{\text{RH}}^2 \approx \rho_R/3m_{\text{pl}}^2$ the radiation energy is predominate. These results depend on the effective degeneracy g_* (7.28) and the decay rate $\tau_R^{-1} = g_Y^2 \hat{m}$ (5.6).

Our numerical calculations show the consistency of the approximation $a_i \lesssim a_R$ used in Eq. (7.30) and the agreement with the analytical solutions (7.31) and (7.33). From Figs. 6 and 7, we find that the reheating predominately takes place around a_R , at which $\tau_R \sim \tau_D$, and the ratios $\tau_R/H_{\text{RH}} \approx \tau_D/H_{\text{RH}} \sim \mathcal{O}(1)$. Moreover, from Fig. 6 (a) we obtain the reheating scale

$$H_{\text{RH}} \approx 3.16 \times 10^{-4} H_{\text{end}} \approx 6.1 \times 10^9 \text{GeV}, \quad a_R \approx 20.1 a_{\text{end}} \quad (7.35)$$

for the case $g_Y^2 = 10^{-9}$ and $\hat{m} = 27.7 m_{\text{pl}}$. We also obtain $H_{\text{RH}} \sim 10^{-1} H_{\text{end}} = 1.9 \times 10^{12} \text{GeV}$ (the plot is not present), and $a_R \approx 1.8 a_{\text{end}}$ for the case $g_Y^2 = 10^{-6}$.

To estimate the the scale factor change a_R/a_{end} in the reheating epoch, we approximately use the conservation law (7.18) for the massive pair domination

$$\Delta_2 \equiv \frac{a_R}{a_{\text{end}}} \approx \left(\frac{\rho_M^i}{\rho_M^f} \right)^{1/3} \approx \frac{1}{\pi} \left(\frac{45}{4} \right)^{1/3} \left(\frac{H_{\text{end}}^2 M_{\text{pl}}^2}{g_* T_{\text{RH}}^4} \right)^{1/3}. \quad (7.36)$$

Here the initial pair energy density $\rho_M^i \approx \rho_\Lambda^{\text{end}} \approx 3m_{\text{pl}}^2 H_{\text{end}}^2$ (6.3) at the beginning of the reheating epoch, and the final one $\rho_M^f \approx \rho_R \approx 3m_{\text{pl}}^2 H_{\text{RH}}^2$ at the end of the reheating epoch, in virtue of Eqs. (7.28) and (7.32).

8 Observations to fix reheating temperature and entropy

We use the method proposed by Ref. [54] to fix the reheating temperature by the CMB observations. The cosmological evolution of the physical wavelength $\lambda(a)$ and wavenumber $k(a)$ is

$$\lambda(a) = \lambda_0 \frac{a}{a_0}, \quad k(a) = k_0 \frac{a_0}{a} \quad \lambda(a) = \frac{1}{k(a)}, \quad (8.1)$$

where the present time $a_0 = 1$, the comoving wavenumber $k(a_0)$ and wavelength $\lambda_0 = 1/k_0$ are constants in the evolution, see Figure 2. The total increase of the scale factor from the horizon crossing a_* (6.1) to a_0 is given by

$$\Delta_{\text{tot}} = \frac{a_0}{a_*} = \frac{\lambda_0}{\lambda(a_*)} = \frac{H_*}{k_0}. \quad (8.2)$$

At the CMB pivot scale $\lambda(a_*) = H_*^{-1} = k_*^{-1}$, the scalar spectrum gives

$$\Delta_{\text{tot}} = \frac{M_{\text{pl}}}{k_*} \sqrt{\pi \epsilon_* A_s} = \frac{M_{\text{pl}}}{\sqrt{2} k_*} \sqrt{\pi(1 - n_s) A_s}. \quad (8.3)$$

On the other hand, as illustrated in Fig. 2 and Ref. [54], $\Delta_{\text{tot}} = \Delta_3 \Delta_2 \Delta_1 \Delta_0$, $\Delta_1 = (a_{\text{rec}}/a_R) = (g_*/2)^{1/3} (T_{\text{RH}}/T_{\text{rec}})$ and $\Delta_0 = (a_0/a_{\text{rec}}) = 1 + z_{\text{rec}}$ are given in terms of the temperature $T_{\text{rec}} = T_{\text{CMB}}(1 + z_{\text{rec}})$ and redshift z_{rec} at the recombination,

$$\Delta_1 \Delta_0 = \frac{a_0}{a_R} \approx (g_*/2)^{1/3} (T_{\text{RH}}/T_{\text{CMB}}). \quad (8.4)$$

Whereas, we compute $\Delta_3 = (a_{\text{end}}/a_*)$ (6.1) and $\Delta_2 = (a_R/a_{\text{end}})$ (7.36) in the $\tilde{\Lambda}$ CDM scenario. As a result, we obtain

$$\Delta_{\text{tot}} = e^{N_{\text{end}}} \frac{1}{\pi} \left(\frac{45}{4} \right)^{1/3} \left(\frac{H_{\text{end}}^2 M_{\text{pl}}^2}{g_* T_{\text{RH}}^4} \right)^{1/3} \frac{T_{\text{RH}}}{T_{\text{CMB}}} \left(\frac{g_*}{2} \right)^{1/3}. \quad (8.5)$$

It agrees with the result (33) using the inflation potential $V(\phi)$ energy density (17) in Ref. [54]. Here we adopt the energy density $\rho_c^{\text{end}} \equiv 3m_{\text{pl}}^2 H_{\text{end}}^2$ (6.3) at inflation end.

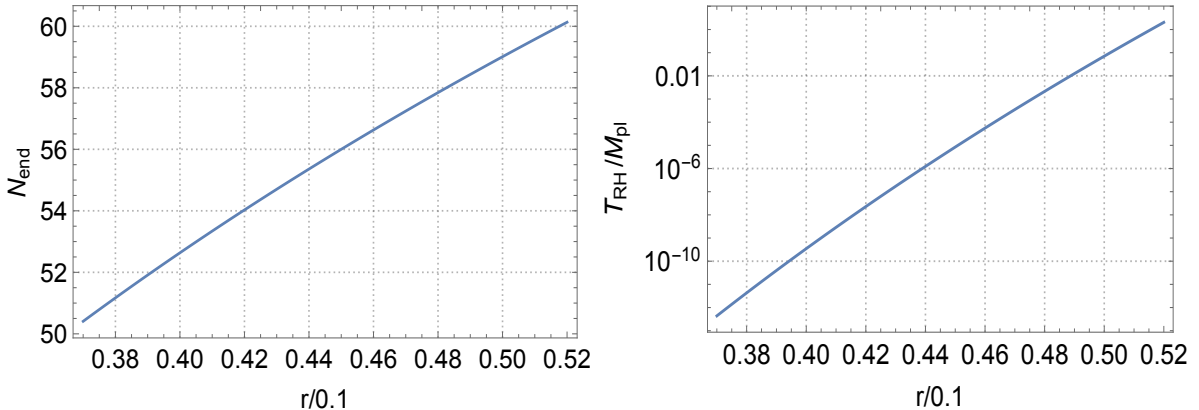


Figure 8. (Color Online). Fixed the observed spectral index $n_s = 0.965$, in terms of the tensor-to-scalar ratio r , we plot the inflation end e -folding number N_{end} (6.2) and the reheating temperature T_{RH} (8.6). These plots refer to their lower limits due to the nature of inequality (6.2). The real values of N_{end} and T_{RH} should be slightly above the curves for a given r value.

Equations (8.3) and (8.5) are independent of the effective reheating degeneracy g_* and yield the reheating temperature

$$\frac{T_{\text{RH}}}{M_{\text{pl}}} = \left(\frac{45}{2^{3/2}} \right) \frac{e^{3N_{\text{end}}}}{\pi^{9/2}} [(1 - n_s)A_s]^{-3/2} \left(\frac{k_*}{T_{\text{CMB}}} \right)^3 \left(\frac{H_{\text{end}}}{M_{\text{pl}}} \right)^2, \quad (8.6)$$

in terms of the CMB observations $T_{\text{CMB}} = 2.725 \text{ K} = 2.348 \times 10^{-4} \text{ eV}$ and $k_* = 0.05 \text{ Mpc}^{-1}$ ($\text{Mpc}^{-1} = 6.39 \times 10^{-30} \text{ eV}$), as well as N_{end} (6.2) and H_{end} (6.1), whose values depend on the CMB measurements A_s , n_s and r , see Sec. 6.

8.1 Reheating temperature and entropy vs tensor-to-scalar ratio $r < 0.048$

Given the observed the scalar amplitude $A_s = 2.1 \times 10^{-9}$ and spectral index $n_s = 0.965$, the inflation ending e -folding number N_{end} (6.1) and the reheating temperature T_{RH} (8.6) are plotted in Fig. 8 as functions of the tensor-to-scalar ratio r without any free parameter. Figure 8 shows that their values are $N_{\text{end}} \approx (50, 60)$ and $T_{\text{RH}}/M_{\text{pl}} \approx (5.5 \times 10^{-13}, 1.1 \times 10^0)$ in the range $r \approx (0.037, 0.052)$.

After obtaining the reheating temperature at the end a_R of reheating, we calculate the entropy S_{patch} produced within the physical patch of the volume H_{RH}^{-3} , which evolves from the initial patch of the volume H_*^{-3} at the start $a_* = 1$ of the inflation. The patch grows by a scale factor of Eqs. (6.1) and (7.36),

$$a_R^3 = (\Delta_3 \Delta_2)^3 \approx \frac{45 e^{3N_{\text{end}}}}{4\pi^3} \left(\frac{H_{\text{end}}^2 M_{\text{pl}}^2}{g_* T_{\text{RH}}^4} \right) = e^{3N_{\text{end}}} \left(\frac{H_{\text{end}}^2}{H_{\text{RH}}^2} \right). \quad (8.7)$$

The entropy per comoving volume S_R (7.34) at the end of reheating is expressed as

$$S_R \approx 2.2 \times 10^6 \left(\frac{16\pi^3}{135} \right)^{1/4} \frac{3a_R^3}{8\pi} H_{\text{end}}^2 M_{\text{pl}}, \quad (8.8)$$

where we use $\rho_M^i(a_i) \approx \rho_\Lambda^{\text{end}} \approx 3m_{\text{pl}}^2 H_{\text{end}}^2$ (7.36) and the constraint (8.11) below. The entropy S_{patch} within the physical patch H_{RH}^{-3} is given by,

$$S_{\text{patch}} = H_{\text{RH}}^{-3} S_R \approx 3.64 \times 10^5 e^{3N_{\text{end}}} \left(\frac{H_{\text{end}}^4 M_{\text{pl}}}{H_{\text{RH}}^5} \right), \quad (8.9)$$

which is a function of r and g_* . In Fig. 9 (right), we plot S_{patch} by using N_{end} (6.2), H_{end} (6.1) and H_{RH} (7.32). It shows the calculated entropy accords with the observational value $S_{\text{patch}} \sim 10^{88}$ around $r \sim 0.045$.

To have a better understanding of how the physical patch horizon $H_* > H_{\text{end}} > H_{\text{RH}}$ evolves, we plot in the same Fig. 9 (left) all characteristic Hubble scales from the inflation to the reheating: the inflation scale H_* , inflation end scale H_{end} (6.1), and reheating scale H_{RH} (7.32) in unit of the Planck scale M_{pl} . It shows that the nonphysical situation $H_{\text{RH}} > H_{\text{end}}$ occurs when $r > 0.047$. Therefore the $r > 0.047$ range excludes. Due to the dependence of H_{RH} on g_* and the approximations adopted in these calculations, we conservatively suggest a theoretical upper limit of the tensor-to-scalar ratio $r < 0.047$. This theoretical upper limit is consistent with the observational one $r < 0.065$ [56], and the recent constraint $r < 0.044$ [57].

In the r -range [0.042, 0.048], we show that (i) the inflation e -folding number $58 \gtrsim N_{\text{end}} \gtrsim 54$ and the reheating temperature $10^{-3} \gtrsim T_{\text{RH}}/M_{\text{pl}} \gtrsim 10^{-8}$ from the numerical results presented in Fig. 8; (ii) the inflation scale $H_*/M_{\text{pl}} \approx 4.0 \times 10^{-6}$, inflation end scale $H_{\text{end}}/M_{\text{pl}} \approx 1.5 \times 10^{-6}$, whereas $10^{-14} \gtrsim H_{\text{RH}}/M_{\text{pl}} \gtrsim 10^{-4}$ and the entropy $10^{120} \gtrsim S_{\text{patch}} \gtrsim 10^{76}$ from the numerical results presented in Fig. 9. These results show that the Λ CDM scenario is consistent with observations. The precisely measuring r -value is essential to determine the e -folding number of the inflation, the reheating temperature, all characteristic Hubble scales and produced entropy.

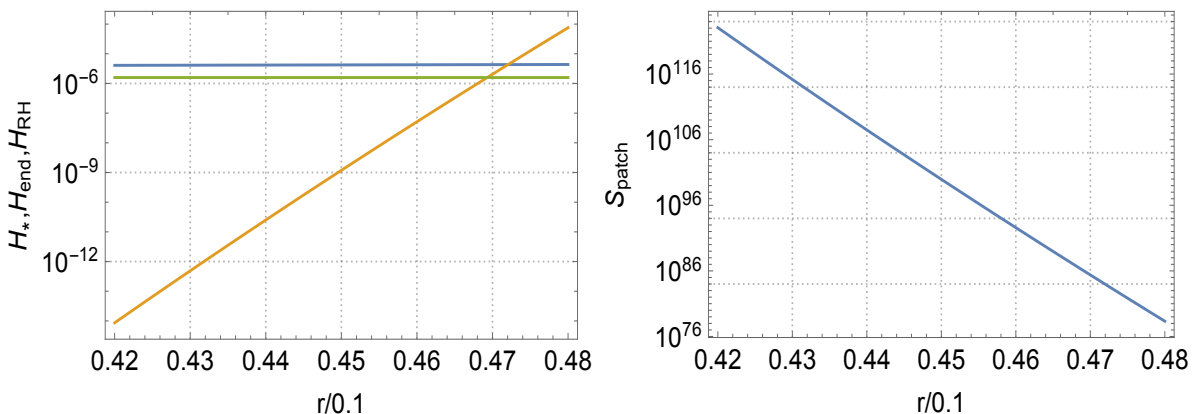


Figure 9. (Color Online). Fixed the observed spectral index $n_s = 0.965$, as functions of the tensor-to-scalar ratio r , we plot (Left) the inflation scale H_* (blue), inflation end scale H_{end} (6.1) (green), and reheating scale H_{RH} (7.32) (orange) in unit of the Planck scale M_{pl} ; (Right) the entropy S_{patch} (8.9) within the physical patch H_{RH}^{-3} at the reheating end a_R . $H_{\text{RH}} \propto g_*^{1/2}$ and $S_{\text{patch}} \propto g_*^{-5/2}$. We adopt $g_* \simeq 10^2$ for the standard model of particle physics, including sterile neutrinos.

8.2 Genuine reheating $\rho_R \gg \rho_M \gg \rho_\Lambda$ and tensor-to-scalar ratio $r > 0$

In the $\tilde{\Lambda}$ CDM scenario, there are two parameters to describe the properties of the reheating epoch: (i) the effective mass parameter \hat{m}/M_{pl} physically represents pairs' masses and numbers; (ii) the effective Yukawa coupling $(g_Y^2/g_*^{1/2})$ represents pairs' decay strength to relativistic particles of degeneracies g_* .

To determine these two parameters, we use Eqs. (7.33) and (8.6) to obtain one constraint,

$$\left(\frac{T_{\text{RH}}}{M_{\text{pl}}}\right)^2 = 0.3 (g_Y^2/g_*^{1/2}) (\hat{m}/M_{\text{pl}}). \quad (8.10)$$

Another constraint is

$$(g_Y^2/g_*^{1/2}) (M_{\text{pl}}/\hat{m}) \approx 3.6 \times 10^{-13}, \quad (8.11)$$

from the reheating temperature T_{RH} (7.33) and the ratio $T_{\text{RH}}/\hat{m} \approx 3.3 \times 10^{-7}$, obtained by the baryon number-to-entropy ratio $n_B/S_R = 0.864_{-0.015}^{+0.016} \times 10^{-10}$ [58], theoretical relation $n_B/S_R \approx \epsilon_{CP}(T_{\text{RH}}/\hat{m})$ [49] and $\epsilon_{CP} \approx 2.6 \times 10^{-4}$, see Eq. (5.3) of Ref. [59].

In Fig. 10, we numerically plot the constraints (8.10) and (8.11) as a function of the tensor-to-scalar ratio r . Recall that in Sec. 7.1.2 we point out the theoretical threshold \hat{m}_{thresh} : $\hat{m} > 20m_{\text{pl}} = 4M_{\text{pl}}$ (7.8) for $\rho_M \gg \rho_\Lambda$. We conclude that the nontrivial threshold \hat{m}_{thresh} demands the tensor-to-scalar ratio $r > 0$, see also Eq. (6.2). Applying the obtained theoretical threshold $\hat{m}_{\text{thresh}} = 4M_{\text{pl}}$ to numerical results Fig. 10, we find that the tensor-to-scalar ratio $r \gtrsim 0.044$. However, it depends on the parameter $\chi \approx 1.85 \times 10^{-3}$ adopted and other approximations used for numerical calculations. To obtain the lower limit $r_{\text{min}} \neq 0$, it requires more elaborated calculations, for example, separating in Eq. (4.1) unstable modes' contribution $\rho_M^H|_{\text{unstable}}$ from stable modes' contribution $\rho_M^H|_{\text{stable}}$ to more accurately determine the mass parameter threshold \hat{m}_{thresh} . Nevertheless, the obtained r -range ($0 < r < 0.047$) is relevant to the measurements by the next generation CMB observations, such as CMB-S4 which measures $r \gtrsim 10^{-3}$ [60].

We report the numerical results in the r range [0.042, 0.048]. The effective pair mass parameter is in $10^{-1} \lesssim \hat{m}/M_{\text{pl}} \lesssim 10^4$ and the effective Yukawa coupling is in $10^{-14} \lesssim (g_Y^2/g_*^{1/2}) \lesssim 10^{-9}$. If $g_* \gtrsim 10^2$ for the standard model of particle physics, including sterile neutrinos, the Yukawa coupling is in the range of $10^{-13} \lesssim g_Y^2 \lesssim 10^{-8}$. We check back the parameters used in Figs. 6 and 7 are $(\hat{m}/m_{\text{pl}}) = 27.7$ and $g_Y^2 = 10^{-9}$. It indicates that the $\tilde{\Lambda}$ CDM scenario is self-consistent and self-contained.

9 Stable massive pairs and cold dark matter abundance

To further clarify dark energy and matter interaction, we study stable massive pairs after reheating. These pairs neither decay into light particles nor contribute to reheating. Thus, they remain and can be candidates for massive cold dark matter (CDM) particles. Here, we qualitatively discuss their evolution after reheating.

In the radiation- and matter-dominated epoch after reheating, the Universe evolution ϵ rate (5.2) is $\epsilon \approx 2$ and $\epsilon \approx 3/2$, respectively. The mean pair-production rate

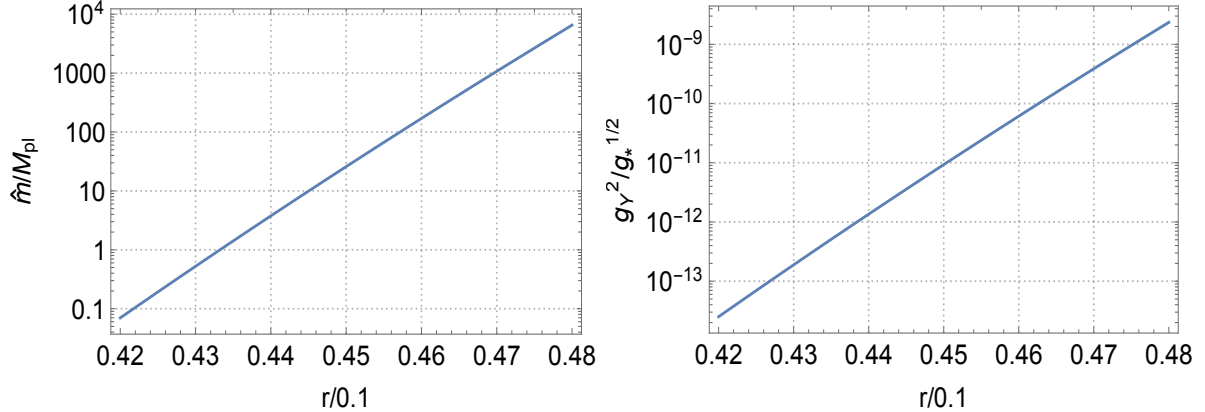


Figure 10. (Color Online). Using the observed spectral index $n_s = 0.965$, we plot the mass parameter \hat{m}/M_{pl} (left) and the effective Yukawa coupling ($g_Y^2/g_*^{1/2}$) (right), as functions of the tensor-to-scalar ratio r in the same range (0.042, 0.048) where the physically sensible values N_{end} and T_{RH} are also plotted in Fig. 8.

(5.1) $\Gamma_M \propto m$ is proportional to the mass parameter m . The large mass m and ratio $\Gamma_M/H > 1$ imply massive stable pairs should tightly couple with dark energy in evolution. Therefore, we focus on stable pairs interacting with dark energy in Eqs. (5.7,5.8), and approximately obtain

$$\frac{d\rho_\Lambda}{dx} \approx -(\Gamma_M/H)(\rho_M^H|_{\text{stable}} - \rho_M^{\text{cold}}), \quad (9.1)$$

$$\frac{d\rho_M^{\text{cold}}}{dx} + 3\rho_M^{\text{cold}} \approx +(\Gamma_M/H)(\rho_M^H|_{\text{stable}} - \rho_M^{\text{cold}}), \quad (9.2)$$

where $\rho_M^H|_{\text{stable}}$ indicates the massive pair plasma state (4.1) for stable pairs. For the coupled case $\Gamma_M/H > 1$, discussed as the case (iii) after Eqs. (5.7,5.8), the approximate solution to Eqs. (9.1,9.2) is

$$\rho_M^{\text{cold}} \approx \rho_M^H|_{\text{stable}} = 2\chi(\hat{m}_M)^2|_{\text{stable}}H^2. \quad (9.3)$$

Equations (9.1,9.2) become

$$\dot{\rho}_\Lambda \approx 0, \quad \dot{\rho}_M^{\text{cold}} + 3H\rho_M^{\text{cold}} \approx -\dot{\rho}_\Lambda, \quad (9.4)$$

with approximate solutions $\rho_M^{\text{cold}} \propto (1/a)^{(3-\delta_M)}$ and $\rho_\Lambda \propto (1/a)^{\delta_\Lambda}$, where indexes $|\delta_{M,\Lambda}| \ll 1$ [18]. It shows massive cold dark matter approximately follows the evolution of non-relativistic fluid, weakly interacting with dark energy. In other words, via massive pair plasma state $\rho_M^H|_{\text{stable}}$, dark energy and cold dark matter interact with each other. However, the exchange between them is small and inefficient. Actually, Eq. (9.3) is essentially the same as Eq. (7.17) and discussions here are similar to the matter-dominated \mathcal{M} -episode of reheating, see Sec. 7.2. One can also find similar discussions [53] that dark energy weakly interacts with radiation and baryon matter, and their exchange is small and inefficient.

Equation (9.3) indicates the cold dark matter abundance Ω_M^{cold} is an approximate constant in time,

$$\Omega_M^{\text{cold}} \approx \Omega_M^H|_{\text{stable}} = \frac{\rho_M^H|_{\text{stable}}}{\rho_c^H} = \frac{16\pi}{3} \chi \left(\frac{\hat{m}_M|_{\text{stable}}}{M_{\text{pl}}} \right)^2, \quad (9.5)$$

where $\rho_c^H \equiv 3H^2/(8\pi G)$. It means that (i) the CDM composes stable massive pairs produced in the pre-reheating \mathcal{P} -episode, see Sec. 7.1; (ii) the current CDM abundance is approximately equal to its abundance in the \mathcal{M} -episode (7.2) of reheating, see Sec. 7.2. The approximate constancy of CDM abundance in time is a direct consequence of the holographic and massive pair plasma state (4.1). To be self-consistent, we give a rough check on the Ω_M^{cold} magnitude by using the theoretical threshold (7.8) $\hat{m}_M|_{\text{stable}}/M_{\text{pl}} \sim \mathcal{O}(10)$ and width parameter $\chi \sim \mathcal{O}(10^{-3})$ constrained by studying inflation [41] and theoretical calculation [39, 40]. It shows the cold dark matter abundance (9.5) can be the right order of the magnitude, compared with the currently observed relic value $\Omega_c^0 \approx 0.3$. This preliminary study requires further detailed investigations. Moreover, as CDM candidates, these massive stable pairs should play some role in primordial black hole formulation and primordial gravitational wave emission.

10 Remarks and summary

10.1 Some remarks

We study the scenario that the cosmological constant term (dark energy) $\Lambda \neq 0$ and $p_\Lambda = -\rho_\Lambda$ represents [63–68] the non-trivial ground state (Wheeler spacetime foam [69]) of the quantum field of spacetime gravity R and R^2 . Dark energy is neither the vacuum energy of quantum fields of particles (matter) nor the energy of the scalar field's kinetics and potential. We need further investigations to understand $p_\Lambda^{\text{fast,slow}} \approx -\rho_\Lambda^{\text{fast,slow}}$ of the spacetime foam interacting to matter. We study in this article the back-and-forth interactions between dark energy and matter via horizon H in the following two aspects.

First, at the scale $\mathcal{O}(1/M)$ for fast components and their back-and-forth reactions, we describe in Sec. 3 the quantum massive pair production and oscillation. It forms a quasi-classical coherent state with a large occupation number of particles. Averaging fast components over microscopic time, we describe the state as a quasi-classical state of massive pair plasma by using a perfect fluid $p_M^H = \omega_M^H \rho_M^H$ in Sec. 4. It is functional of dark energy $p_\Lambda^{\text{slow}} \approx -\rho_\Lambda^{\text{slow}}$ and normal matter $p_{R,M} = \omega_{R,M} \rho_{R,M}$ via the horizon.

Second, at the scale $\mathcal{O}(1/H)$ for slow components and their interactions, we discuss in Sec. 5 the macroscopic back-and-forth interacting system between the classical pair plasma fluid ρ_M^H , normal matter fluids $\rho_{R,M}$, dark energy $p_\Lambda^{\text{slow}} \approx -\rho_\Lambda^{\text{slow}}$ and horizon H_{slow} via nonlinear Eqs. (6.6–6.9). The novel cosmic rate equation (6.8) accounts for the massive pair plasma state interacting with dark energy and normal matter. The system yields $\tilde{\Lambda}$ CDM scenario that describes inflation, reheating and standard cosmology.

In Ref. [41], we study $\tilde{\Lambda}$ -driven inflation in detail, compare and contrast it with usual canonical inflation models of the scalar field ϕ , potential $V(\phi)$, Friedman equation $3m_{\text{pl}}^2 H^2 = \dot{\phi}^2/2 + V(\phi)$, energy density $\rho_\phi = \dot{\phi}^2/2 + V(\phi)$ and pressure $p_\phi = \dot{\phi}^2/2 - V(\phi)$. The correspondences between inflation models and the $\tilde{\Lambda}$ -driven inflation

$$\dot{\phi}^2 \Leftrightarrow \rho_M^H + p_M^H \quad V(\phi) \Leftrightarrow \rho_\Lambda + (\rho_M^H - p_M^H)/2, \quad (10.1)$$

where the dark energy density ρ_Λ is an $\mathcal{O}(1/H)$ slow component. The $\mathcal{O}(1/M)$ fast oscillating component $\rho_\Lambda^{\text{fast}}$ has no relation to the classical field ϕ . The slow-roll condition $V(\phi) \gg \dot{\phi}^2/2$ corresponds to $\rho_\Lambda \gg \rho_M^H$ for $\rho_M^H \approx (2\chi m^2/3m_{\text{pl}}^2)\rho_\Lambda$. It leads to $\dot{\rho}_\Lambda \Leftrightarrow \dot{V} = \dot{\phi}V'$ and $\dot{\rho}_M^H \Leftrightarrow (1/2)d(\dot{\phi}^2)/dt = \dot{\phi}\ddot{\phi}$. Equation (2.3), namely Eq. (5.1) in Ref. [41], corresponds to the classical equation of motion for ϕ : $\ddot{\phi} + 3H\dot{\phi} + V'(\phi) = 0$. In inflation, we approximately obtain an analytical solution by neglecting the cosmic rate equation (5.5) because of $\rho_M^H \gg \rho_{R,M}$. In reheating, we have to numerically solve the Friedman equations, cosmic rate equation and reheating equation (6.6-6.9), which yield a complex back-and-forth reaction system of inter-playing three scales τ_H, τ_M, τ_D and τ_R dynamics.

10.2 Summary

We make a summary to close this lengthy article. In the ρ_Λ -dominated inflation $H > \Gamma_M$, where the massive pair plasma density ρ_M^H is small and normal matter density ρ_M is negligible. The reheating epoch starts $\Gamma_M > H$, ρ_M^H and ρ_M become large, and their back reaction and decay to relativistic particles are important. Therefore, the cosmic rate equation (5.5) governing the processes $\rho_M^H \Leftrightarrow \rho_M$ (5.3) and unstable massive pairs' decay $\bar{F}F \rightarrow \bar{\ell}\ell$ are relevant. It is an additional dynamical equation to two Friedman equations (2.2,2.3) and the reheating equation (5.10) from energy conservation.

Using the massive pair plasma density ρ_M^H (6.5), production rate Γ_M and decay rate Γ_M^{de} (6.10), we study the reheating epoch by a close system of four dynamical (ordinary differential equations) equations (6.6-6.9) for the horizon H and three densities $\rho_{\Lambda,M,R}$. The initial conditions are given by the inflation end. Numerically solving this system, we find three characteristic episodes:

- (i) the \mathcal{P} -episode of the transition from the inflation end to the reheating start, when the pair-production rate is much larger than the Hubble rate ($\Gamma_M \gg H$), the dark energy density ρ_Λ quickly decreases and converts to the matter-energy density ρ_M . As a consequence $\rho_\Lambda \ll \rho_M$;
- (ii) the \mathcal{M} -episode of massive pairs domination, where the back-and-forth interaction of the cosmic rate equation (5.5) plays an essential role, and dark energy density slowly varies;
- (iii) the \mathcal{R} -episode of the genuine reheating $\rho_R \gg \rho_M$, when unstable massive pairs predominately decay to relativistic particles that quickly thermalised.

We emphasise the pair mass threshold $\hat{m} > \hat{m}_{\text{thresh}}$ (7.8) that at the pre-reheating start $\rho_\Lambda \gg \rho_M \gg \rho_R$, the rapid converting process $\rho_\Lambda \Rightarrow \rho_M \Rightarrow \rho_R$ leads to $\rho_\Lambda \ll \rho_M \ll \rho_R$. The most relevant mass-energy and entropy of Universe are produced by the end of reheating. Such dynamic processes should lead to the emission of primordial gravitational waves [61, 62].

The initial conditions for the reheating epoch are the Hubble scale H_{end} and energy densities $\rho_{\Lambda, M}^{\text{end}}$ at the end of inflation after e -folding number N_{end} . They are determined by the CMB measurements of scalar amplitude A_s and spectral index n_s at pivot scale $k_* = 0.05(\text{Mpc})^{-1}$ and the Hubble scale H_* [41]. We obtain the reheating Hubble scale H_{RH} , temperature T_{RH} and entropy S_{patch} at the genuine reheating episode. They are functions of the tensor-to-scalar ratio r , and their numerical values are in accordance with the CMB observations. Moreover, from purely theoretical viewpoints, we preliminarily limit the r values in the range $0 < r < 0.047$. Among massive pairs gravitationally produced, (i) unstable pairs decay to relativistic particles, accounting for reheating; (ii) stable pairs couple only to gravity and are candidates for cold dark matter. The resultant cold dark matter abundance $\Omega_c \sim 10^{-1}$ is about a constant in time. They should play the role in the formation of primordial black holes.

11 Acknowledgment

The author thanks the EPJC Editor Alexei Starobinsky and anonymous referees for their reviews and reports that give chances to improve the manuscript.

12 Appendix: Quantum pair oscillation details

In microscopic time, we plot the Bogoliubov coefficient $|\beta|^2$, the quantum pair density $\varrho_\Lambda^{\text{fast}}$ and pressure $\mathcal{P}_\Lambda^{\text{fast}}$, as well as the fast components of Hubble function h_{fast} , and cosmological term $\varrho_\Lambda^{\text{fast}}$. Recall $\mathcal{P}_\Lambda^{\text{fast}} \approx -\varrho_\Lambda^{\text{fast}}$.

References

- [1] A. A. Starobinsky, *A new type of isotropic cosmological models without singularity*, *Phys. Lett. B* **91** (1980) 99.
- [2] A. H. Guth, *The inflationary universe: A possible solution to the horizon and flatness problems*, *Phys. Rev. D* **23** (1981) 347.
- [3] A. D. Linde, *A new inflationary universe scenario: A possible solution of the horizon, flatness, homogeneity, isotropy and primordial monopole problems*, *Phys. Lett. B* **108** (1982) 389–393.
- [4] V. F. Mukhanov and G. V. Chibisov, *The vacuum energy and large scale structure of the universe*, *Sov. Phys. JETP* **56** (1982) 258–265.
- [5] A. Albrecht and P. J. Steinhardt, *Cosmology for grand unified theories with radiatively induced symmetry breaking*, *Phys. Rev. Lett.* **48** (1982) 1220.

- [6] A. D. Linde, *Chaotic inflation*, *Phys. Lett. B* **129** (1983) 177.
- [7] R. Kallosh and A. Linde, *BICEP/Keck and cosmological attractors*, *JCAP* **12** (2021) 008 [[2110.10902](#)].
- [8] L. Kofman, A. D. Linde and A. A. Starobinsky, *Reheating after inflation*, *Phys. Rev. Lett.* **73** (1994) 3195 [[hep-th/9405187](#)].
- [9] L. Kofman, A. D. Linde and A. A. Starobinsky, *Towards the theory of reheating after inflation*, *Phys. Rev. D* **56** (1997) 3258 [[hep-ph/9704452](#)].
- [10] Y. Shtanov, J. H. Traschen and R. H. Brandenberger, *Universe reheating after inflation*, *Phys. Rev. D* **51** (1995) 5438 [[hep-ph/9407247](#)].
- [11] B. A. Bassett and S. Liberati, *Geometric reheating after inflation*, *Phys. Rev. D* **58** (1998) 021302 [[hep-ph/9709417](#)].
- [12] S. Tsujikawa, K.-I. Maeda and T. Torii, *Resonant particle production with nonminimally coupled scalar fields in preheating after inflation*, *Phys. Rev. D* **60** (1999) 063515 [[hep-ph/9901306](#)].
- [13] D. I. Podolsky and A. A. Starobinsky, *Chaotic reheating*, *Grav. Cosmol. Suppl.* **8N1** (2002) 13 [[astro-ph/0204327](#)].
- [14] R. Allahverdi, R. Brandenberger, F.-Y. Cyr-Racine and A. Mazumdar, *Reheating in inflationary cosmology: Theory and applications*, *Ann. Rev. Nucl. Part. Sci.* **60** (2010) 27 [[1001.2600](#)].
- [15] M. A. Amin, R. Easther, H. Finkel, R. Flauger and M. P. Hertzberg, *Oscillons after inflation*, *Phys. Rev. Lett.* **108** (2012) 241302 [[1106.3335](#)].
- [16] M. A. Amin, M. P. Hertzberg, D. I. Kaiser and J. Karouby, *Nonperturbative dynamics of reheating after inflation: A review*, *Int. J. Mod. Phys. D* **24** (2014) 1530003 [[1410.3808](#)].
- [17] P. Adshead, J. T. Giblin, M. Pieroni and Z. J. Weiner, *Constraining axion inflation with gravitational waves across 29 decades in frequency*, *Phys. Rev. Lett.* **124** (2020) 171301 [[1909.12843](#)].
- [18] S.-S. Xue, *How universe evolves with cosmological and gravitational constants*, *Nucl. Phys. B* **897** (2015) 326 [[1410.6152](#)].
- [19] L. Parker, *Particle creation in expanding universes*, *Phys. Rev. Lett.* **21** (1968) 562.
- [20] L. Parker, *Quantized fields and particle creation in expanding universes. II*, *Phys. Rev. D* **3** (1971) 346.
- [21] L. Parker, *Quantized fields and particle creation in expanding universes. I*, *Phys. Rev.* **183** (1969) 1057.

- [22] Y. B. Zeldovich and A. A. Starobinsky, *Particle production and vacuum polarization in an anisotropic gravitational field*, *JETP [Zh. Eksp. Teor. Fiz.* **61** (1971) 2161-2175] **34** (1972) 1159.
- [23] L. Parker and S. A. Fulling, *Quantized matter fields and the avoidance of singularities in general relativity*, *Phys. Rev. D* **7** (1973) 2357.
- [24] V. M. M. S. G. Mamaev and A. A. Starobinsky, *Particle production and vacuum polarization in an anisotropic gravitational field*, *JETP* **43** (5) (1976) 823.
- [25] Y. B. Zeldovich and A. A. Starobinsky, *Rate of particle production in gravitational fields*, *JETP Lett.* **26**, 252-255 (1977) **26** (1977) 252.
- [26] A. A. Starobinsky, *Spectrum of relict gravitational radiation and the early state of the universe*, *JETP Lett.* **30** (1979) 682.
- [27] N. D. Birrell and P. C. W. Davies, *Quantum Fields in Curved Space*, Cambridge Monographs on Mathematical Physics. Cambridge Univ. Press, Cambridge, UK, 2, 1984, [10.1017/CBO9780511622632](https://doi.org/10.1017/CBO9780511622632).
- [28] E. Mottola, *Particle creation in De Sitter space*, *Phys. Rev. D* **31** (1985) 754.
- [29] S. Habib, C. Molina-Paris and E. Mottola, *Energy momentum tensor of particles created in an expanding universe*, *Phys. Rev. D* **61** (2000) 024010 [[gr-qc/9906120](https://arxiv.org/abs/gr-qc/9906120)].
- [30] P. R. Anderson and E. Mottola, *Instability of global De Sitter space to particle creation*, *Phys. Rev. D* **89** (2014) 104038 [[1310.0030](https://arxiv.org/abs/1310.0030)].
- [31] P. R. Anderson and E. Mottola, *Quantum vacuum instability of “eternal” De Sitter space*, *Phys. Rev. D* **89** (2014) 104039 [[1310.1963](https://arxiv.org/abs/1310.1963)].
- [32] A. Landete, J. Navarro-Salas and F. Torrenti, *Adiabatic regularization and particle creation for spin one-half fields*, *Phys. Rev. D* **89** (2014) 044030 [[1311.4958](https://arxiv.org/abs/1311.4958)].
- [33] A. A. Starobinsky, *Nonsingular model of the universe with the quantum-gravitational de sitter stage and its observational consequences*, *Proc. of the Second Seminar “Quantum Theory of Gravity”, Moscow, October 1981*, INR Press, Moscow (1982) 58.
- [34] L. H. Ford, *Gravitational particle creation and inflation*, *Phys. Rev. D* **35** (1987) 2955.
- [35] E. W. Kolb, A. D. Linde and A. Riotto, *Gut baryogenesis after preheating*, *Phys. Rev. Lett.* **77** (1996) 4290 [[hep-ph/9606260](https://arxiv.org/abs/hep-ph/9606260)].
- [36] D. J. H. Chung, P. Crotty, E. W. Kolb and A. Riotto, *On the gravitational production of superheavy dark matter*, *Phys. Rev. D* **64** (2001) 043503 [[hep-ph/0104100](https://arxiv.org/abs/hep-ph/0104100)].
- [37] D. J. H. Chung, E. W. Kolb and A. J. Long, *Gravitational production of super-hubble-mass particles: an analytic approach*, *JHEP* **01** (2019) 189 [[1812.00211](https://arxiv.org/abs/1812.00211)].
- [38] Y. Ema, K. Nakayama and Y. Tang, *Production of purely gravitational dark matter*, *JHEP* **09** (2018) 135 [[1804.07471](https://arxiv.org/abs/1804.07471)].

- [39] S.-S. Xue, *Cosmological Λ driven inflation and produced massive particles*, [1910.03938](#).
- [40] S.-S. Xue, *Cosmological constant, matter, cosmic inflation and coincidence*, *Mod. Phys. Lett. A* **35** (2020) 2050123 [[2004.10859](#)].
- [41] S.-S. Xue, *Massive particle pair production and oscillation in Friedman universe: its effect on inflation*, *Eur. Phys. J. C* **83** (2023) 36 [[2112.09661](#)].
- [42] D. Bégué, C. Stahl and S.-S. Xue, *A model of interacting dark fluids tested with supernovae and baryon acoustic oscillations data*, *Nucl. Phys. B* **940** (2019) 312 [[1702.03185](#)].
- [43] L. Parker and S. A. Fulling, *Adiabatic regularization of the energy-momentum tensor of a quantized field in homogeneous spaces*, *Phys. Rev. D* **9** (1974) 341.
- [44] Y. Kluger, J. M. Eisenberg, B. Svetitsky, F. Cooper and E. Mottola, *Pair production in a strong electric field*, *Phys. Rev. Lett.* **67** (1991) 2427.
- [45] R. Ruffini, G. Vereshchagin and S.-S. Xue, *Electron-positron pairs in physics and astrophysics: from heavy nuclei to black holes*, *Phys. Rept.* **487** (2010) 1 [[0910.0974](#)].
- [46] G. 't Hooft, *Dimensional reduction in quantum gravity*, *Conf. Proc. C* **930308** (1993) 284 [[gr-qc/9310026](#)].
- [47] L. Susskind, *The world as a hologram*, *J. Math. Phys.* **36** (1995) 6377 [[hep-th/9409089](#)].
- [48] A. G. Cohen, D. B. Kaplan and A. E. Nelson, *Effective field theory, black holes, and the cosmological constant*, *Phys. Rev. Lett.* **82** (1999) 4971 [[hep-th/9803132](#)].
- [49] E. W. Kolb and M. S. Turner, *The Early Universe*, vol. 69. 1990, [10.1201/9780429492860](#).
- [50] B. W. Lee and S. Weinberg, *Cosmological lower bound on heavy neutrino masses*, *Phys. Rev. Lett.* **39** (1977) 165.
- [51] R. Ruffini, J. D. Salmonson, J. R. Wilson and S. S. Xue, *On the evolution of the pair-electromagnetic pulse of a charged black hole*, *Astron. Astrophys* **138**, 511-512 (1999) **138** (1999) 511 [[astro-ph/9905021](#)].
- [52] R. Ruffini, J. D. Salmonson, J. R. Wilson and S.-S. Xue, *On the pair-electromagnetic pulse from an electromagnetic black hole surrounded by a baryonic remnant*, *Astron. Astrophys* **359**, 855-864 (2000) (2000) [[astro-ph/0004257](#)].
- [53] S.-S. Xue, *Massive particle pair production and oscillation in Friedman universe: dark energy and matter interaction*, [2203.11918](#).
- [54] J. Mielczarek, *Reheating temperature from the CMB*, *Phys. Rev. D* **83** (2011) 023502 [[1009.2359](#)].

- [55] PLANCK collaboration, *Planck 2018 results. VI. cosmological parameters*, *Astron. Astrophys.* **641** (2020) A6 [[1807.06209](#)].
- [56] PLANCK collaboration, *Planck 2018 results. X. constraints on inflation*, *Astron. Astrophys.* **641** (2020) A10 [[1807.06211](#)].
- [57] M. Tristram et al., *Planck constraints on the tensor-to-scalar ratio*, *Astron. Astrophys.* **647** (2021) A128 [[2010.01139](#)].
- [58] PLANCK collaboration, *Planck 2015 results. XIII. cosmological parameters*, *Astron. Astrophys.* **594** (2016) A13 [[1502.01589](#)].
- [59] S.-S. Xue, *Horizon crossing causes baryogenesis, magnetogenesis and dark-matter acoustic wave*, [2007.03464](#).
- [60] K. Abazajian et al., *CMB-S4 science case, reference design, and project plan*, [1907.04473](#).
- [61] M. Maggiore, *Gravitational wave experiments and early universe cosmology*, *Phys. Rept.* **331** (2000) 283 [[gr-qc/9909001](#)].
- [62] M. C. Guzzetti, N. Bartolo, M. Liguori and S. Matarrese, *Gravitational waves from inflation*, *Riv. Nuovo Cim.* **39** (2016) 399 [[1605.01615](#)].
- [63] Sidney R. Coleman, *Why There Is Nothing Rather Than Something: A Theory of the Cosmological Constant*, *Nucl. Phys. B* **310** (1988) 643–668 [DOI: [10.1016/0550-3213\(88\)90097-1](#)].
- [64] A. O. Barvinsky, *Why there is something rather than nothing (out of everything)?*, *Phys. Rev. Lett.* **99** (2007) 071301 [[hep-th/0704.0083](#)].
- [65] S.-S. Xue, *Gravitational instanton and cosmological term*, *Int. J. Mod. Phys. A* **24** (2009) 3865–3891 [[hep-th/0608220](#)].
- [66] S.-S. Xue, *Detailed discussions and calculations of quantum Regge calculus of Einstein-Cartan theory*, *Phys. Rev. D* **82** (2010) 064039 [[0912.2435](#)].
- [67] S.-S. Xue, *Quantum Regge calculus of Einstein-Cartan theory*, *Phys. Lett. B* **682** (2009) 300 [[0902.3407](#)].
- [68] S.-S. Xue, *The phase and critical point of quantum Einstein-Cartan gravity*, *Phys. Lett. B* **711** (2012) 404 [[1112.1323](#)].
- [69] Charles W. Misner and K. S. Thorne and J. A. Wheeler, *Gravitation*, 1990, W. H. Freeman publisher, ISBN 978-0-7167-0344-0, 978-0-691-17779-3.

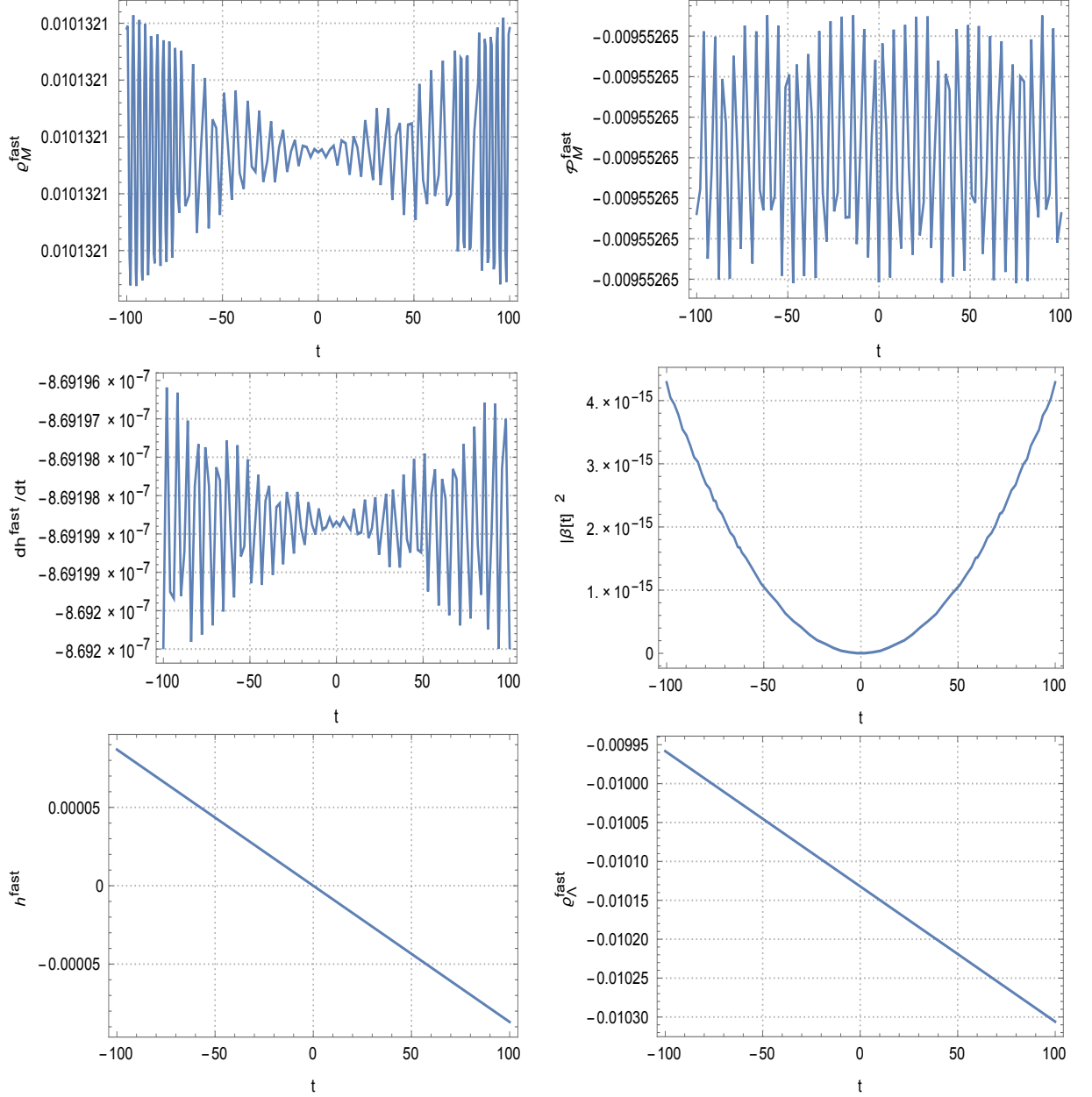


Figure 11. Corresponding to Fig. 1, the details of quantum pair oscillation are shown in microscopic time t in the unit of M^{-1} . The parameters' values are the same as those in Fig. 1. The non-smooth curve $|\beta(t)|^2$ shows its oscillating behavior. The h_{fast} and $\varrho_{\Lambda}^{\text{fast}}$ oscillatory structures are too small to see due to the precision limit for numerical calculations with the parameters' values used. However, one can infer their oscillating behaviours by the oscillating dh^{fast}/dt shown and fast-component Eqs. (3.11). We suggest readers see Fig. 4 of Ref. [41] for pre-inflation and inflation, where the corresponding solutions for other parameters' values and plotting scales show evident oscillatory structures. The quantum pressure $\mathcal{P}_M^{\text{fast}}$ and its time average are negative.